Published in final edited form as:

Cell Rep. 2022 October 04; 41(1): 111434. doi:10.1016/j.celrep.2022.111434.

Molecular mechanism of RIPK1 and caspase-8 in homeostatic type I interferon production and regulation

Yaqiu Wang[1], **Rajendra Karki**[1], **Raghvendra Mall**[1], **Bhesh Raj Sharma**[1], **Ravi C. Kalathur**[2], **SangJoon Lee**[1], **Balabhaskararao Kancharana**[1], **Matthew So**[1], **Katie L. Combs**[1], **Thirumala-Devi Kanneganti**[1,3,*]

[1]Department of Immunology, St. Jude Children's Research Hospital, Memphis, TN 38105, USA

[2]Department of Structural Biology, St. Jude Children's Research Hospital, Memphis, TN 38105, USA

[3]Lead contact

SUMMARY

Type I interferons (IFNs) are essential innate immune proteins that maintain tissue homeostasis through tonic expression and can be upregulated to drive antiviral resistance and inflammation upon stimulation. However, the mechanisms that inhibit aberrant IFN upregulation in homeostasis and the impacts of tonic IFN production on health and disease remain enigmatic. Here, we report that caspase-8 negatively regulates type I IFN production by inhibiting the RIPK1-TBK1 axis during homeostasis across multiple cell types and tissues. When caspase-8 is deleted or inhibited, RIPK1 interacts with TBK1 to drive elevated IFN production, leading to heightened resistance to norovirus infection in macrophages but also early onset lymphadenopathy in mice. Combined deletion of caspase-8 and RIPK1 reduces the type I IFN signaling and lymphadenopathy, highlighting the critical role of RIPK1 in this process. Overall, our study identifies a mechanism to constrain tonic type I IFN during homeostasis which could be targeted for infectious and inflammatory diseases.

Graphical Abstract

*Correspondence: thirumala-devi.kanneganti@stjude.org.

AUTHOR CONTRIBUTIONS

Y.W., R.K., and T.-D.K. conceptualized the study; Y.W. and R.K. designed the methodology; Y.W., R.K., B.R.S., R.C.K., S.L., B.K., and M.S. performed the experiments; R.M. conducted the gene expression and publicly available dataset analysis; K.L.C. analyzed *in vivo* data; Y.W. wrote the manuscript with input from all the authors; and T.-D.K. acquired the funding and provided overall supervision.

SUPPLEMENTAL INFORMATION

Supplemental information can be found online at https://doi.org/10.1016/j.celrep.2022.111434.

DECLARATION OF INTERESTS

T.-D.K. is a consultant for Pfizer.

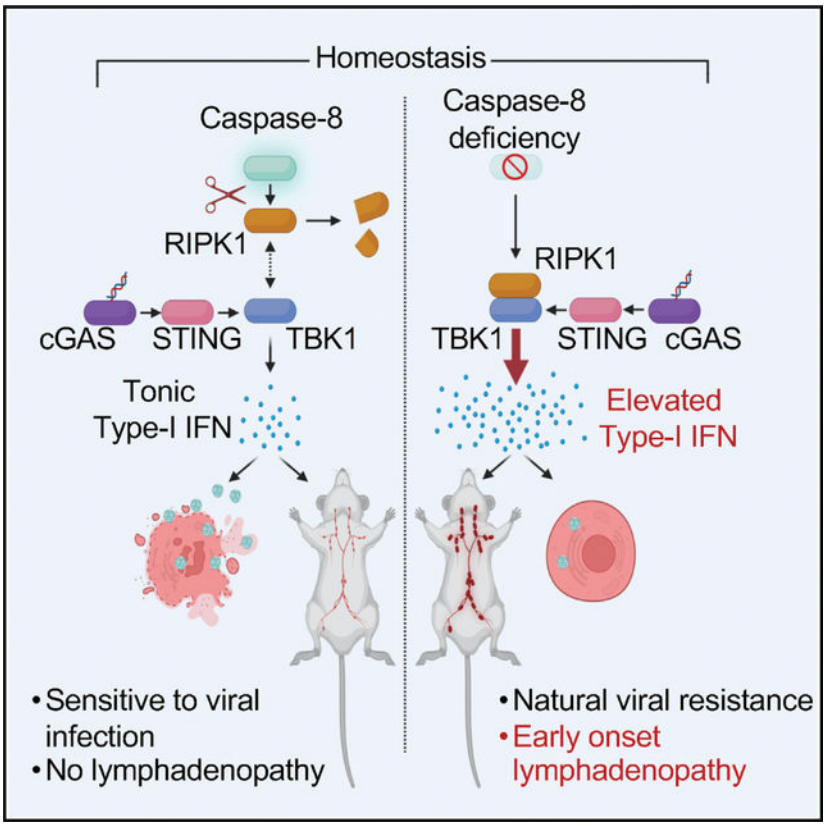

In brief

Wang et al. report the mechanistic regulation of homeostatic type I IFN production by caspase-8 through the RIPK1-TBK1 axis. Hyper-activation of this pathway due to loss of caspase-8 has profound physiological impacts on natural resistance to viral infection and the pathogenesis of lymphadenopathy.

INTRODUCTION

Type I interferons (IFNs) are key molecules in innate immunity, the first line of defense against infection and sterile insults. In response to microbial or endogenous DNA or RNA, pattern recognition receptors initiate signaling pathways, including cGAS-STING, RIG-I/MDA5-MAVS, and TLR3/4, that upregulate type I IFNs. These pathways each activate TBK1, which phosphorylates IRF3/7 and allows for their nuclear translocation to induce type I IFN transcription (Fitzgerald et al., 2003). Type I IFNs signal in an autocrine and paracrine manner by binding IFNAR1 and IFNAR2 to initiate JAK-STAT signaling (e.g., STAT1 phosphorylation) to promote IFN-stimulated gene (ISG) transcription and establish an antiviral cellular state (Ivashkiv and Donlin, 2014) by interfering with viral replication (McNab et al., 2015).

Type I IFNs are also produced at low levels during homeostasis (Gough et al., 2012). This “tonic” production allows cells to quickly respond to and resist pathogens and regulates host susceptibility to viral infection (Barrat et al., 2019; Gough et al., 2012; Liu et al.,

2018; Marie et al., 2021; Sarhan et al., 2019; Stefan et al., 2020; Xing et al., 2016). Tight regulation of type I IFNs is crucial, as overproduction disrupts homeostasis and causes unwanted immune responses and inflammation (Crow et al., 2019; Ivashkiv and Donlin, 2014). Therefore, it is important to understand mechanisms affecting homeostatic type I IFN production.

Caspases are critical regulators of inflammation, cell death, and type I IFN production (Kesavardhana et al., 2020). In apoptosis, caspases-9 and -3 suppress cGAS-STING-mediated type I IFN production (Rongvaux et al., 2014; White et al., 2014). During viral infection, caspase-8 and executioners caspases-3 and -7 suppress type I IFN production (Chen et al., 2017; Ning et al., 2019; Rajput et al., 2011). However, the role of caspases in regulating homeostatic type I IFN signaling has not been clearly established. Caspase-8 has a key role in inflammation; its loss is linked to overproduction of proinflammatory cytokines as well as autoinflammatory syndromes (Kang et al., 2018) and a chronic skin inflammatory disease associated with constitutive IRF3 signaling (Kovalenko et al., 2009). While caspase-8 inhibits type I IFN signaling (Kang et al., 2018; Lalaoui et al., 2020; Newton et al., 2019a), the physiological function of enhanced homeostatic IFN production in the absence of caspase-8 and the underlying molecular mechanism have not been studied.

Here, we discovered that the loss of caspase-8 elevated homeostatic type I IFN production, providing naturally enhanced resistance to viral infections. Type I IFN signaling was elevated across multiple caspase-8-deficient cell types and tissues *in vitro* and *in vivo*. Without caspase-8, its proteolytic substrate RIPK1 interacted with TBK1, promoting TBK1 phosphorylation in a RIPK1 kinase-dependent manner to enhance homeostatic type I IFN production. This hyper-activated type I IFN signaling increased antiviral resistance through reduced inflammasome activation and inflammatory cell death and induced early onset lymphadenopathy. Loss of RIPK1 or neutralization of type I IFN blocked these phenotypes. Our findings identify caspase-8 and RIPK1 as regulators of tonic type I IFN production, elucidating molecular mechanisms and infectious and inflammatory disease relevance that deepen our understanding of tissue homeostasis, viral resistance, and autoimmunity.

RESULTS

Caspase-8 regulates tonic type I IFN production

Caspase-8 has many roles in regulating inflammation (Tummers and Green, 2017). Embryonic lethality and skin inflammation caused by caspase-8 deficiency in mice can be rescued by ablation of necroptosis (e.g., crossing with *Ripk3*$^{-/-}$), highlighting the well-established role of caspase-8 in regulating necroptosis. Yet, *Casp8*$^{-/-}$*Ripk3*$^{-/-}$ mice still develop autoinflammation, including lymphadenopathy, by 4 months of age (Kaiser et al., 2011; Oberst et al., 2011). We hypothesized that caspase-8 has roles in homeostasis beyond inhibiting necroptosis. To test this, we performed a microarray analysis using primary bone marrow-derived macrophages (BMDMs) from *Casp8*$^{-/-}$*Ripk3*$^{-/-}$ and *Ripk3*$^{-/-}$ mice. An unbiased gene set enrichment analysis (GSEA) (Subramanian et al., 2005) showed that type I IFN signaling was the most highly enriched pathway in *Casp8*$^{-/-}$*Ripk3*$^{-/-}$ versus *Ripk3*$^{-/-}$ BMDMs (Figure 1A). We obtained similar results re-analyzing publicly available RNA sequencing (RNA-seq) data comparing untreated *Casp8*$^{-/-}$*Ripk3*$^{-/-}$ and

Ripk3$^{-/-}$ BMDMs (Figures S1A and S1B; GEO: GSE86922; Philip et al., 2016). Type I IFN hyper-activation was also observed in colon tissue when caspase-8 was deleted in intestinal epithelial cells (Figure 1B; GEO: GSE137281) (Schwarzer et al., 2020). In agreement, STAT1 phosphorylation (pSTAT1), a marker of activated type I IFN signaling, was increased in untreated *Casp8*$^{-/-}$*Ripk3*$^{-/-}$ BMDMs compared with *Ripk3*$^{-/-}$ BMDMs (Figure 1C). Total STAT1 was increased in *Casp8*$^{-/-}$*Ripk3*$^{-/-}$ BMDMs (Figure 1C), as there is a positive feedback loop further inducing STAT1 expression as a result of type I IFN activation (Lehtonen et al., 1997). Consistently, the amount of IFNβ in supernatant was significantly increased in *Casp8*$^{-/-}$*Ripk3*$^{-/-}$ BMDMs compared with wild-type (WT) and *Ripk3*$^{-/-}$ BMDMs (Figure 1D). Treatment with an anti-IFNAR1 antibody reduced pSTAT1 in *Casp8*$^{-/-}$*Ripk3*$^{-/-}$ cells to the level seen in *Ripk3*$^{-/-}$ and WT cells, confirming that the STAT1 upregulation was due to type I IFN signaling (Figure 1E). These data show that caspase-8 regulates homeostatic tonic type I IFN production and signaling *in vivo* and *in vitro*.

Because type I IFN production is important in responding to infection (Barrat et al., 2019; Gough et al., 2012; Liu et al., 2018; Marie et al., 2021; Sarhan et al., 2019; Stefan et al., 2020; Xing et al., 2016), we examined the effects of type I IFN hyper-activation when caspase-8 is ablated during murine norovirus (MNV-1) infection. Myeloid cells are susceptible to MNV-1 (Van Winkle et al., 2018), and intact type I IFN signaling is required for host protection (Karst et al., 2003). While WT BMDMs were susceptible to MNV-1-induced cell death, cells deficient in *Stat1* or *Ifnar1* were hyper-susceptible, and priming WT BMDMs with IFNβ provided resistance to cell death (Figures 1F and 1G). MNV-1 replicated in WT and *Ripk3*$^{-/-}$ BMDMs, as indicated by increased amounts of MNV-1 capsid protein (cp), while *Casp8*$^{-/-}$*Ripk3*$^{-/-}$ BMDMs had lower amounts of MNV-1 cp (Figure 1H). In agreement, WT and *Ripk3*$^{-/-}$ BMDMs were susceptible to MNV-1 infection-induced cell death, while caspase-8-deficient BMDMs were resistant (Figures 1I and 1J), phenocopying IFNβ-primed WT cells (Figures 1F and 1G). Therefore, elevated homeostatic type I IFN is functional and confers viral resistance to *Casp8*$^{-/-}$*Ripk3*$^{-/-}$ BMDMs.

Caspase-8 plays both enzymatic and scaffolding roles in signaling (Orning and Lien, 2021); its protease function is important for activation and the cleavage of executioner caspases (Hughes et al., 2009), while its scaffolding function is required for NLRP3 inflammasome activation (Gurung et al., 2014; Kang et al., 2015). To determine if caspase-8 enzymatic activity was required to regulate tonic type I IFN signaling, we analyzed publicly available single-cell RNA-seq data from mouse embryos with enzymatically inactive caspase-8 (*Casp8*^{CA}; GEO: GSE132133) (Newton et al., 2019b). Enterocytes, stromal cells, and phagocytes all showed enhancement of the type I IFN signature (Figures S1C–S1H), showing that the enzymatic activity of caspase-8 is critical to suppress type I IFN hyperactivation in homeostasis.

RIPK1 mediates type I IFN upregulation in the absence of caspase-8

We next sought to elucidate the downstream mechanism of caspase-8-mediated suppression of homeostatic type I IFN production. Caspase-8 enzymatic activity suppresses necroptosis

by cleaving RIPK1 during homeostasis (Newton et al., 2019a) and initiates extrinsic apoptosis by activating executioner caspases (Hughes et al., 2009). Using BMDMs from *Fadd*$^{-/-}$*Ripk3*$^{-/-}$ mice and mice carrying an autoprocessing-deficient version of caspase-8 (*Casp8*$^{D387A/D387A}$; *Casp8*$^{DA/DA}$) (Wang et al., 2021), we tested whether caspase-8 enzymatic activity-mediated cleavage of RIPK1 was required for homeostatic type I IFN suppression. FADD is required to mediate the caspase-8-RIPK1 interaction; this interaction is compromised in *Fadd*$^{-/-}$*Ripk3*$^{-/-}$ mice (Lin et al., 1999), while the CASP8$^{DA/DA}$ mutant retains RIPK1 cleavage activity (Oberst et al., 2011; Pop et al., 2011). *Fadd*$^{-/-}$*Ripk3*$^{-/-}$ cells phenocopied *Casp8*$^{-/-}$*Ripk3*$^{-/-}$ cells with enhanced STAT1 phosphorylation during homeostasis, while pSTAT1 remained basal in *Casp8*$^{DA/DA}$ cells (Figure 2A), implicating RIPK1 function in this process. Deleting *Ripk1* with *Casp8* and *Ripk3* rescued the enhanced STAT1 phosphorylation seen in *Casp8*$^{-/-}$*Ripk3*$^{-/-}$ cells (Figure 2B). Similarly, increased expression of *Ifnb1* and ISGs (*Cxcl10* and *Zbp1*) seen in *Casp8*$^{-/-}$*Ripk3*$^{-/-}$ BMDMs was reduced upon *Ripk1* ablation (Figure 2C). Microarray analysis showed that the enrichment of the type I IFN gene signature and overexpression of many ISGs in *Casp8*$^{-/-}$*Ripk3*$^{-/-}$ cells were rescued in *Casp8*$^{-/-}$*Ripk3*$^{-/-}$*Ripk1*$^{-/-}$ cells (Figures 2D and 2E). Consistent with previous findings (Kang et al., 2018), expression of some cytokines (such as *Tnf* and *Il3*) was also modulated in response to caspase-8 ablation in a RIPK1-dependent manner (Figure 2D).

RIPK1 also has enzymatic and scaffolding functions (Malireddi et al., 2018, 2020). We did not observe increased total RIPK1 expression in *Casp8*$^{-/-}$*Ripk3*$^{-/-}$ cells, but there was increased autophosphorylation at S166 in *Casp8*$^{-/-}$*Ripk3*$^{-/-}$ cells (Figure 2F). Treating *Casp8*$^{-/-}$*Ripk3*$^{-/-}$ BMDMs with Nec-1s prevented STAT1 hyper-phosphorylation in *Casp8*$^{-/-}$*Ripk3*$^{-/-}$ BMDMs (Figure 2G), implicating RIPK1 kinase activity in regulating type I IFN production. Adding exogenous IFNβ along with Nec-1s induced similar STAT1 phosphorylation in WT, *Casp8*$^{-/-}$*Ripk3*$^{-/-}$, *Ripk3*$^{-/-}$, and *Casp8*$^{-/-}$*Ripk3*$^{-/-}$*Ripk1*$^{-/-}$ BMDMs, indicating that RIPK1 functions upstream of the type I IFN receptor (Figure 2G). Indeed, RIPK1 ablation or kinase inhibition significantly reduced IFNβ production in *Casp8*$^{-/-}$*Ripk3*$^{-/-}$ cells (Figure 2H). Together, these data show that RIPK1 upregulates type I IFN production and signaling in the absence of caspase-8.

STING is required for RIPK1-mediated type I IFN production during caspase-8 deficiency

Caspase-8 is thought to regulate other caspases in addition to caspases-3 and −7 (Tummers and Green, 2017). Therefore, we tested whether other caspases modulate type I IFN signaling by analyzing STAT1 phosphorylation in untreated BMDMs from different caspase-deficient mice. We found hyper-phosphorylated STAT1 and increased IFNβ in *Casp8*$^{-/-}$*Ripk3*$^{-/-}$ cells and *Casp3*$^{-/-}$ cells (Figures 1D, S2A and S2B). Additionally, untreated fetal liver-derived macrophages (FLDMs) from *Casp9*$^{-/-}$ mice had hyper-phosphorylated STAT1 compared with WT FLDMs (Figure S2C). These findings are consistent with the reported function of the CASP9-CASP3 axis in suppressing cGAS-STING-driven type I IFN production (Rongvaux et al., 2014; White et al., 2014).

Treatment with the STING inhibitor H151 reduced STAT1 phosphorylation in WT cells treated with the STING agonist diA-BZI and in naive *Casp3*$^{-/-}$ and *Casp9*$^{-/-}$ cells (Figures

S2C–S2E). STING inhibition also blocked STAT1 phosphorylation in *Casp8*$^{-/-}$*Ripk3*$^{-/-}$ cells (Figure S2E), suggesting shared molecular features for type I IFN regulation in caspase-8- and −3-deficient cells. However, inhibiting RIPK1 kinase activity reduced STAT1 phosphorylation in *Casp8*$^{-/-}$*Ripk3*$^{-/-}$ cells (Figures 2G and S2E) but not in *Casp3*$^{-/-}$ or *Casp9*$^{-/-}$ cells (Figures S2C and S2E), suggesting that RIPK1 is critical in STING-mediated type I IFN production when caspase-8 is absent but not in cas-pase-9- or -3-deficient cells.

RIPK1 interacts with TBK1 and promotes its activation in the absence of caspase-8

Given RIPK1's ability to drive aberrant type I IFN production in caspase-8-deficient cells, we next investigated RIPK1's function in regulating type I IFNs. We stimulated BMDMs with c-di-GMP transfection, poly(I:C) transfection, or poly(I:C) treatment, which selectively activate cGAS-STING, RIG-I/MDA5-MAVS, and TLR3/4-TRIF pathways, respectively. Caspase-8 deficiency enhanced STAT1 phosphorylation in response to each treatment, while combined caspase-8 and RIPK1 deletion reduced STAT1 phosphorylation or returned it to baseline (Figure S3A). These data suggest RIPK1-dependent activation of type I IFN signaling in caspase-8-deficient cells occurs through a process shared by the cGAS-STING, RIG-I/MDA5-MAVS, and TLR3/4-TRIF pathways. In BMDMs expressing a kinase-dead version of RIPK1, *Ripk1*$^{K45A/K45A}$ (*Ripk1* KD), loss of RIPK1 kinase activity had no effect on homeostatic type I IFN responses nor in response to these ligands (Figure S3B). Therefore, RIPK1 promotes the activation of type I IFN signaling only in the absence of caspase-8.

In the cGAS-STING, RIG-I/MDA5-MAVS, and TLR3/4-TRIF pathways, phosphorylation of adaptor molecules by TBK1 precedes IRF3 phosphorylation and type I IFN transcription (McNab et al., 2015). *Casp8*$^{-/-}$*Ripk3*$^{-/-}$ BMDMs also had increased TBK1 phosphorylation compared with WT BMDMs (Figure 3A). Similarly, increased STAT1 and TBK1 phosphorylation were seen in *Casp8*$^{-/-}$*Mlkl*$^{-/-}$ BMDMs (Figure 3B), further implicating caspase-8 and suggesting a role for TBK1 in type I IFN suppression. Treatment with the TBK1 inhibitor GSK8612 reduced STAT1 phosphorylation in caspase-8-deficient cells (Figures 3C and 3D), similar to the effect of Nec-1s (Figure 2G), suggesting that RIPK1 and TBK1 function in the same pathway to promote type I IFN production in *Casp8*$^{-/-}$*Ripk3*$^{-/-}$ cells. To delineate the relationship between RIPK1 and TBK1, we examined TBK1 phosphorylation in *Casp8*$^{-/-}$*Ripk3*$^{-/-}$ and *Casp8*$^{-/-}$*Ripk3*$^{-/-}$*Ripk1*$^{-/-}$ cells with and without Nec-1s. RIPK1 and its kinase activity were required to promote increased TBK1 phosphorylation in the absence of caspase-8 (Figure 3E), suggesting that RIPK1 may promote TBK1 activation. Further, treating WT cells with the pan-caspase inhibitor z-VAD increased TBK1 and STAT1 phosphorylation in a RIPK1 kinase-dependent manner (Figures 3F and 3G). Furthermore, RIPK1 and TBK1 were co-immunoprecipitated more robustly in caspase-8-deficient BMDMs compared with BMDMs where caspase-8 was expressed (Figure 3H). Overexpressing human RIPK1 in HEK293T cells also resulted in an interaction with endogenous TBK1 (Figure S4A).

RIPK1 is cleaved by caspase-8 in homeostasis (Lalaoui et al., 2020), and that cleavage is attenuated in *Casp8*$^{-/-}$*Ripk3*$^{-/-}$ cells (Figure 2F). We found that full-length RIPK1 bound TBK1 (Figure S4A, B), but the N-terminal RIPK1 fragment (amino acids 1–324; containing

the kinase domain) generated by caspase-8 cleavage did not (Figure S4B). Instead, RIPK1 bound TBK1 through its C-terminal domains (amino acids 325–671; containing its RHIM and death domain) (Figure S4B). We also generated a RIPK1 mutant that is resistant to caspase-8-mediated cleavage to confirm the role of the RIPK1 kinase domain in TBK1 activation. While overexpressing WT RIPK1 induced TBK1 phosphorylation, having uncleavable RIPK1 further increased TBK1's phosphorylation (Figure S4C), suggesting that without caspase-8, RIPK1 interacts with TBK1 and promotes TBK1 phosphorylation to drive homeostatic type I IFN production.

RIPK1 suppresses norovirus-induced cell death in caspase-8-deficient cells

Given the viral resistance observed in *Casp8*$^{-/-}$*Ripk3*$^{-/-}$ BMDMs during MNV-1 infection (Figures 1H–1J) and the role for RIPK1 in type I IFN hyper-activation when caspase-8 is ablated, we examined if RIPK1-mediated type I IFN signaling caused the viral resistance in *Casp8*$^{-/-}$*Ripk3*$^{-/-}$ cells. Neutralizing IFNAR1 restored MNV-1 infection-induced cell death in *Casp8*$^{-/-}$*Ripk3*$^{-/-}$ cells (Figures 4A and 4B), establishing a causal link between type I IFN signaling and the viral resistance associated with caspase-8 deficiency. Additionally, deletion of *Ripk1* along with *Casp8* and *Ripk3* restored the sensitivity to MNV-1-induced cell death (Figures 4C and 4D) and allowed increased MNV-1 replication in *Casp8*$^{-/-}$*Ripk3*$^{-/-}$*Ripk1*$^{-/-}$ cells compared with *Casp8*$^{-/-}$*Ripk3*$^{-/-}$ cells (Figures 4E and 4F). Additionally, RIPK1-dependent hyper-phosphorylation of TBK1 in *Casp8*$^{-/-}$*Ripk3*$^{-/-}$ cells occurred during MNV-1 infection (Figure 4F). Further, the activation of biochemical markers of pyroptosis and apoptosis induced by MNV-1 in WT cells was decreased in *Casp8*$^{-/-}$*Ripk3*$^{-/-}$ cells but restored in *Casp8*$^{-/-}$*Ripk3*$^{-/-}$*Ripk1*$^{-/-}$ cells (Figure 4G), implicating inflammasomes and PANoptosis, a unique innate immune inflammatory cell death pathway regulated by PANoptosomes that integrate components from other cell death pathways (Christgen et al., 2020; Gullett et al., 2022; Karki et al., 2021a, 2021b, 2022; Kuriakose et al., 2016; Lee et al., 2021; Zheng et al., 2020), in this process. These data indicate that RIPK1-mediated type I IFN production supports the intrinsic antiviral defense in the absence of caspase-8 and that MNV-1-induced cell death occurs without caspase-8, RIPK3, and RIPK1.

RIPK1 and type I IFN promote lymphadenopathy in young mice lacking caspase-8

Although embryonic lethality of caspase-8 deletion in mice is rescued by deleting RIPK3 (Kaiser et al., 2011; Oberst et al., 2011), *Casp8*$^{-/-}$*Ripk3*$^{-/-}$ mice still develop autoinflammation and lymphadenopathy, as do caspase-8-deficient patients (Chun et al., 2002). RIPK1 partially contributes to lymphadenopathy in aged *Casp8*$^{-/-}$*Ripk3*$^{-/-}$ mice (Dillon et al., 2014; Rickard et al., 2014). As caspase-8 and RIPK1 both contribute to tonic type I IFN signaling, and type I IFNs cause lymphocyte retention in the lymph nodes during viral infections (Kamphuis et al., 2006; Shiow et al., 2006), we investigated the effects of RIPK1 on pathology in *Casp8*$^{-/-}$*Ripk3*$^{-/-}$ mice. The lymph nodes and spleens were comparable in size in young WT and *Casp8*$^{-/-}$*Ripk3*$^{-/-}$*Ripk1*$^{-/-}$ mice but were enlarged in age- and sex-matched *Casp8*$^{-/-}$*Ripk3*$^{-/-}$ mice (Figure 5A). Spleen weight was significantly reduced in *Casp8*$^{-/-}$*Ripk3*$^{-/-}$*Ripk1*$^{-/-}$ mice compared with *Casp8*$^{-/-}$*Ripk3*$^{-/-}$ mice (Figure 5B). Splenic and peripheral lymph node lysates showed enhanced TBK1 and IRF3 phosphorylation in *Casp8*$^{-/-}$*Ripk3*$^{-/-}$ mice (Figures 5C and 5D), confirming that the type I

IFN production pathway was activated *in vivo*. Additionally, IFNβ was barely detectable in WT tissue lysates but was observed in spleen and lymph nodes of *Casp8*$^{-/-}$*Ripk3*$^{-/-}$ mice (Figures 5C and 5D). Similarly, STAT1 phosphorylation was increased in *Casp8*$^{-/-}$*Ripk3*$^{-/-}$ tissue lysates. Additionally, the activation of the type I IFN production pathway and downstream signaling were reduced to WT levels in *Casp8*$^{-/-}$*Ripk3*$^{-/-}$*Ripk1*$^{-/-}$ spleen and lymph node lysates (Figures 5C and 5D).

Given the increased IFNβ in *Casp8*$^{-/-}$*Ripk3*$^{-/-}$ mouse tissues (Figures 5C and 5D), we sought to establish a causal link between type I IFN and lymphadenopathy. We treated *Casp8*$^{-/-}$*Ripk3*$^{-/-}$ mice with neutralizing antibodies against IFNβ or immunoglobulin G (IgG) for 6 weeks, starting at 4 weeks of age (Figure S5A). IFNβ neutralization decreased type I IFN signaling in the lymph nodes and spleen (Figure S5B). Additionally, lymph node and spleen sizes in *Casp8*$^{-/-}$*Ripk3*$^{-/-}$ mice were reduced after anti-IFNβ treatment (Figures S5C and S5D). Together, these data suggest RIPK1 has a major role in the pathogenesis of lymphadenopathy by upregulating type I IFN signaling in caspase-8-deficient mice.

DISCUSSION

Although caspase-8-deficient embryonic lethality in mice is rescued by deleting *Ripk3*, *Casp8*$^{-/-}$*Ripk3*$^{-/-}$ mice still develop inflammatory symptoms and lymphadenopathy (Kaiser et al., 2011; Oberst et al., 2011). When using this model, the potential for epistatic effects from *Ripk3* deletion in *Casp8*$^{-/-}$*Ripk3*$^{-/-}$ mice must be considered when drawing conclusions about caspase-8 functions. By analyzing data from multiple caspase-8-deficient systems (i.e., *Casp8*$^{-/-}$*Ripk3*$^{-/-}$, *Casp8*$^{-/-}$*Mlkl*$^{-/-}$, *Casp8*^{CA}*Mlkl*$^{-/-}$, and *Vil1*-cre × *Casp8*$^{fl/fl}$) and comparing to their respective controls, we showed caspase-8 suppressed homeostatic type I IFN. Other caspases regulate type I IFN production via cGAS-STING, RIG-I/MDA5-MAVS, and TLR3/4-TRIF pathways and IRF3 (Chen et al., 2017; Ning et al., 2019), but we found that the absence of caspase-8 in homeostasis allowed a RIPK1-TBK1 interaction to drive type I IFN hyperactivation.

Homeostatic type I IFN was reported to result from cell-intrinsic activation of the cGAS-STING pathway (Rongvaux et al., 2014; White et al., 2014). Indeed, we observed that the caspase-8-suppressed, RIPK1-facilitated type I IFN production was also mediated by STING, suggesting that the caspase-8/RIPK1 axis is a new regulatory layer downstream of cGAS-STING. Our data suggest that this contributes to the early onset of lymphadenopathy in caspase-8-deficient mice. While lymphadenopathy develops later in *Casp8*$^{-/-}$*Ripk3*$^{-/-}$ and *Casp8*$^{-/-}$*Ripk3*$^{-/-}$*Ripk1*$^{-/-}$ mice due to a cell death defect caused by loss of caspase-8 and RIPK3, aged *Casp8*$^{-/-}$*Ripk3*$^{-/-}$*Ripk1*$^{-/-}$ mice have milder symptoms than *Casp8*$^{-/-}$*Ripk3*$^{-/-}$ mice (Dillon et al., 2014; Rickard et al., 2014), suggesting that RIPK1 contributes to the disease independent of cell death. This effect is most prominent in younger (<10 weeks old) mice; at this time, *Casp8*$^{-/-}$*Ripk3*$^{-/-}$*Ripk1*$^{-/-}$ mice appear normal but *Casp8*$^{-/-}$*Ripk3*$^{-/-}$ mice develop disease. IFNs cause lymphocyte retention in the lymph nodes during viral infection (Kamphuis et al., 2006; Shiow et al., 2006), and IFNβ neutralization reduced lymph node size in *Casp8*$^{-/-}$*Ripk3*$^{-/-}$ mice, suggesting that IFNs play a critical role in pathology at this early age. Lymphadenopathy is also observed in humans with homozygous catalytically inactive caspase-8 (Chun et al., 2002) or heterozygous

caspase-8 cleavage-resistant RIPK1 mutations (Lalaoui et al., 2020). Our findings suggest that elevated homeostatic type I IFN may play a role in these diseases.

The caspase-8/RIPK1 axis also caused resistance to norovirus infection. Pan-caspase inhibitor treatment efficiently activated the RIPK1-TBK1 pathway and upregulated type I IFN signaling. Evidence suggests that the FDA-approved pan-caspase inhibitor Emricasan may be effective in viral infections, such as chronic hepatitis C virus (Shiffman et al., 2010) and Zika virus (Xu et al., 2016), though its mechanism of action remains undefined. Based on our results, caspase-8 inhibition through treatment with Emricasan may be a promising strategy to prevent certain viral infections.

While the RIPK1-TBK1 interaction downstream of death-receptor engagement disables RIPK1-mediated cell death (Taft et al., 2021; Xu et al., 2018), our study suggests that such interaction conversely promotes TBK1 activation in the absence of caspase-8 in a RIPK1 kinase-dependent manner. TBK1 *trans*-autophosphorylates upon oligomerization (Zhang et al., 2019). Studies have shown that RIPK1 kinase activity promotes self-oligomerization and complex formation with RIPK3 (Chen et al., 2022; Orozco et al., 2014). Given that RIPK1 and TBK1 interacted under caspase-8-deficient conditions, the kinase activity of RIPK1 could promote the oligomerization of endogenous RIPK1 in homeostasis and enhance TBK1 oligomerization and subsequent autophosphorylation. Further investigation of such a possibility and the impacts of RIPK1 kinase activity on other pathways (e.g., TNF signaling, ZBP1 expression and function) in caspase-8-deficient cells is needed.

As TBK1 can activate the nuclear factor κB (NF-κB) pathway and induce proinflammatory cytokine expression (Pomerantz and Baltimore, 1999), the RIPK1-TBK1 axis may be involved in proinflammatory cytokine production observed in caspase-8-deficient mice (Kang et al., 2018) and in humans with cleavage-resistant RIPK1 (Lalaoui et al., 2020). Overall, our results highlight the regulation of spontaneous type I IFN production by the RIPK1-TBK1 axis when caspase-8 is absent, shedding new light on the mechanism governing tonic type I IFN and suggesting new treatment strategies for patients with pathologies in this pathway.

Limitations of the study

Here, we showed that caspase-8 suppressed homeostatic type I IFN production by regulating the RIPK1-TBK1 axis. Though we showed RIPK1 upstream of TBK1, how RIPK1 is activated remains unknown. TNF signaling, STING, or ZBP1 may serve as potential activators. Further, due to the prominent role of type I IFNs in inflammatory diseases, we focused on their signaling throughout our study. Yet, other proinflammatory cytokines (e.g., TNF) are also upregulated in caspase-8-deficient cells. Their function, regulation, and crosstalk with type I IFNs in pleiotropic caspase-8 deficiency have not been examined. Additionally, our study used mice, where caspase-8 is the only initiator caspase for extrinsic apoptosis. Given that humans also express caspase-10 as an initiator caspase, the situation in humans is likely more complex. Mutations in human caspase-10 (Wang et al., 1999) or caspase-8 (Chun et al., 2002) can cause autoimmune lymphoproliferative syndromes. While we observed that human RIPK1 and TBK1 interacted, it is unknown how human caspase-8 and/or caspase-10 contribute to regulation of the RIPK1-TBK1 axis.

STAR★METHODS

Detailed methods are provided in the online version of this paper and include the following:

RESOURCE AVAILABILITY

Lead contact—Further information and requests for reagents may be directed to and will be fulfilled by the lead contact, Thirumala-Devi Kanneganti (thirumala-devi.kanneganti@stjude.org).

Materials availability—All unique reagents generated in this study are available from the lead contact in accordance with the relevant material transfer agreements.

Data and code availability

- The previously published microarray data can be accessed in GEO under accession numbers GSE137281; GSE86922; GSE132133 and are publicly available as of the date of publication. All other datasets generated or analyzed during this study are included in the published article and deposited in GEO under the accession number GSE211623.
- All software and packages applied are publicly available and listed in the key resources table. The specific analysis parameters used are explained in the STAR Methods section. This paper does not report original code.
- Any additional information required to reanalyze the data reported in this paper is available from the lead contact upon reasonable request.

EXPERIMENTAL MODEL AND SUBJECT DETAILS

Mice—C57Bl6 wildtype (WT) mice, *Casp8*$^{-/-}$*Ripk3*$^{-/-}$ (Oberst et al., 2011), *Fadd*$^{-/-}$*Ripk3*$^{-/-}$ (Dillon et al., 2012), *Ripk3*$^{-/-}$ (Newton et al., 2004), *Casp8*$^{D387A/D387A}$ (Wang et al., 2021), *Ripk1*$^{K45A/K45A}$ (*Ripk1* KD) (Berger et al., 2014) *Ticam1*$^{-/-}$ (Yamamoto et al., 2003), *Mavs*$^{-/-}$ (Kumar et al., 2006; Suthar et al., 2010), *Sting*$^{gt/gt}$ (Sauer et al., 2011), *Stat1*$^{-/-}$ (Durbin et al., 1996), *Ifnar1*$^{-/-}$ (Muller et al., 1994), *Casp1*$^{-/-}$ (Man et al., 2016), *Casp2*$^{-/-}$ (Jackson Laboratory, 007899 (Bergeron et al., 1998)), *Casp3*$^{-/-}$ (Zheng et al., 2000), *Casp6*$^{-/-}$ (Jackson Laboratory, 006236 (Zheng et al., 2020)), *Casp7*$^{-/-}$ (Lakhani et al., 2006), *Casp9*$^{-/-}$ (Hakem et al., 1998), *Casp11*$^{-/-}$ (Kayagaki et al., 2011), *Casp12*$^{-/-}$ (Vande Walle et al., 2016) mice have been described previously. *Casp8*$^{-/-}$*Ripk3*$^{-/-}$*Ripk1*$^{-/-}$ were created by crossing *Casp8*$^{-/-}$*Ripk3*$^{-/-}$ and *Ripk1*$^{-/-}$ mice, which have been described previously (Kelliher et al., 1998; Oberst et al., 2011). For IFNβ neutralization in *Casp8*$^{-/-}$*Ripk3*$^{-/-}$ mice, 500 μg anti-IFNβ (Leinco, I-439) was intraperitoneally injected twice a week starting at the age of four weeks and continuing for six weeks. For comparison, WT mice were injected with saline or IFNβ (1 μg; PBL Assay, 12400-1). Animal studies were conducted under protocols approved by the St. Jude Children's Research Hospital Committee on the Use and Care of Animals.

Cell culture—Primary BMDMs were cultured from mouse tibia and femur extrudes for 6 days in BMDM medium (IMDM [Thermo Fisher Scientific, 12440-053] supplemented with

10% FBS [Biowest, S1620], 30% L929-conditioned medium, 1% non-essential amino acids [Thermo Fisher Scientific, 11140-050] and 1% penicillin and streptomycin [Thermo Fisher Scientific, 15070-063]). Additional medium was supplemented at day 3 and day 5.

METHOD DETAILS

Cell stimulation—BMDMs were seeded into 12-well plates (Corning, 3513) at a density of 1 million cells per well and incubated overnight before stimulations or treatments with the following reagents where indicated: GSK8612 (Selleckchem, S8872); H151 (Selleckchem, S6652); Nec-1s (Selleckchem, S8641); poly(I:C) (for extracellular stimulation, InvivoGen, tlrl-picw); poly(I:C) (for transfection, InvivoGen, tlrl-pic); diABZI (Selleckchem, S8796); c-di-GMP (InvivoGen, tlrl-nacdg); IFNβ (PBL Assay, 12400-1); anti-IFNAR1 (MAR1-5A3, Invitrogen, 16-5945-85);, LPS (Sigma, L2630); or z-VAD-FMK (Cayman, 14463). Transfection was performed using Xfect transfection reagent (Takara, 631318) according to the manufacturer's instructions. Fetal liver derived macrophages (FLDMs) were differentiated from fetal liver cells collected at embryonic day E14.5 and cultured with the same protocol as BMDMs.

Infections—Murine norovirus (MNV-1) CW1 strain was obtained from ATCC (VR-1937) and amplified in RAW264.7 (ATCC TIB-71) macrophages as reported (Hwang et al., 2014). The virus was purified by centrifugation at 30,000 × g for 3 h, and viral titer was determined by plaque assay in RAW264.7 cells. For *in vitro* infection, viral adsorption (MNV-1 MOI = 10) was done in plain DMEM (Sigma, D6171) containing 1% penicillin and streptomycin. The media was supplemented with FBS to reach 10% FBS 2 h after adding virus for further culture and downstream analyses.

Real-time cell death analysis—IncuCyte S3 or SX5 imaging systems (Sartorius) were used for real-time cell death assays. BMDMs were seeded in 12-well plates (10^6 BMDMs/well) and stimulated as indicated. SYTOX Green (100 nM; Thermo Fisher Scientific, S7020) was added after viral adsorption. The images were acquired every 1 h at 37°C and 5% CO_2. The resulting images were analyzed, and SYTOX Green-positive cells were quantified using the software package provided with the IncuCyte instrument.

Immunoblot—Immunoblotting was performed as previously described (Zheng et al., 2020). In brief, for signaling analysis, the BMDM supernatants were removed at the indicated time points, and cells were washed once with PBS, after which cells were lysed with RIPA buffer (1% NP-40, 150 mM NaCl, Tris-HCl 50 mM, 1% sodium deoxycholate, 0.1% SDS, 1× protease inhibitors [Sigma, S8820], 1× phosphatase inhibitors [Roche PHOSS-RO]). For caspase analysis, BMDMs were lysed along with the supernatant using 50 μL caspase lysis buffer (1× protease inhibitors, 1× phosphatase inhibitors, 10% NP-40, and 25 mM DTT) followed by the addition of 100 μL 4× SDS loading buffer. Proteins from lymph nodes and spleen were extracted using RIPA buffer, and 30 μg protein per lane was loaded on the gel. Proteins were separated by electrophoresis through 8%–12% polyacrylamide gels. Following electrophoretic transfer of proteins onto PVDF membranes (Millipore, IPVH00010), non-specific binding was blocked by incubation with 5% skim milk; then membranes were incubated with primary antibodies overnight at

4°C. The primary antibodies used were: anti–MNV-1 cp (Sigma, MABF2097-100UG, 1:1000), anti–phospho-STAT1 (Cell Signaling Technology [CST], #7649, 1:1000), anti-STAT1 (CST, #14994, 1:1000), anti–phospho-TBK1 (CST, #5483, 1:1000), anti-TBK1 (CST, #3504, 1:1000), anti–phospho-RIPK1 (CST, #65746, 1:1000), anti-RIPK1 (CST, #3493, 1:1000), anti–phospho-IRF3 (CST, #29047, 1:1000), anti-IRF3 (CST, #4302, 1:1000), anti–caspase-8 (CST, #4790, 1:1000), anti-RIPK3 (ProSci, #2283, 1:1000), anti-FLAG (Rockland, #600-401-383, 1:3000), anti-HA (Millipore, 05-904, 1:1000), anti–caspase-1 (AdipoGen, AG-20B-0042, 1:1000), anti–caspase-3 (CST, #9662, 1:1000), anti-cleaved caspase-3 (CST, #9661, 1:1000), anti–caspase-7 (CST, #9492, 1:1000), anti-cleaved caspase-7 (CST, #9491, 1:1000), anti-GSDMD (Abcam, ab209845, 1:1000), anti-GSDME (Abcam, ab215191, 1:1000), anti-mouse IFNβ (Leico, MIB-5E9.1, 5 μg/mL) and anti–β-actin (Proteintech, 66009-1-IG, 1:5000). Then the membrane was washed in TBST (Tris-Buffered Saline with 0.05% Tween-20) and incubated with HRP-conjugated secondary antibodies (Jackson ImmunoResearch Laboratories, anti-rabbit [111-035-047], 1:5000; anti-mouse [315-035-047], 1:5000) at room temperature for 1 h. Blot images were developed by using Luminata Forte Western HRP Substrate (Millipore, WBLUF0500), and acquired with an Amersham imager, then analyzed with ImageJ (v1.53a).

Overexpression and immunoprecipitation (IP)—HEK293T cell were seeded into 6-well plates, and 2 μg of Flag-RIPK1 (Addgene #78842) was transfected using Xfect transfection reagent (Takara, 631318) in OptiMEM medium (Gibco, #31985070) and incubated at 37°C and 5% CO_2 for 4 h. DMEM containing 10% FBS and 1% penicillin and streptomycin was added after aspiration of transfection medium, then the cells were incubated for 48 h. Cells were then washed once with PBS, lysed with 300 μL lysis buffer (1% NP-40, 150 mM NaCl, 50 mM Tris-HCl pH 7.2, 1 mM Na_3VO_4, 10 mM β-glycerophosphate, 50 μg/mL PMSF with SIGMA FAST protease inhibitor) and placed on ice for 20 min and centrifuged at 12,000 × g for 10 min. The lysate was incubated with 3 μL anti-Flag antibody (SIGMA, F3165) or anti-HA antibody (Thermo, PA1-985) on gentle rotation overnight at 4°C. Then 50 μL protein A/G agarose beads (SantaCruz sc-2003) were washed with lysis buffer and mixed with lysate on gentle rotation for 3 h at 4°C. Beads were washed with 1 mL lysis buffer 4 times, and 50 μL 2× SDS-PAGE loading dye was added before boiling at 95°C for 5 min and immunoblotting. For endogenous IP, 600 μL lysate from 10^7 BMDMs were prepared with the same procedure, and anti-TBK1 antibody (CST, #3504, 1:100) was added for overnight rotation. Bead binding and washing conditions were the same as those used for FLAG IP. Truncations of human RIPK1 were PCR amplified and cloned by HiFi assembly (NEB, E5520S) into pcDNA with HA tag (Addgene, #128034). Human RIPK1 mutant D325/301A was generated by site-directed mutagenesis with vector PCR and subsequent DpnI digestions, as previously described (Bala Bhaskara Rao et al., 2019).

Enzyme-linked immunosorbent assay (ELISA)—BMDM medium was replaced with DMEM containing 10% FBS (Biowest, S1620) and 1% penicillin and streptomycin 24 h before supernatant collection. Then, the supernatant was used to measure IFNβ by ELISA (BioLegend, #439407) according to the manufacturer's instruction.

Real-time qPCR analysis—RNA was extracted by TRIzol (Invitrogen, 15596026) and reverse transcribed to cDNA using the High-Capacity cDNA Reverse Transcription Kit (Applied Biosystems, 4368814). Real-time PCR was performed on an ABI 7500 real-time PCR instrument with 2× SYBR Green (Applied Biosystems, 4367659). Primer sequences used in this study were as follows: 5′-CAGCTCCAAGAAAGGACGAAC-3′ and 5′-GGCAGTGTAACTCTTCTGCAT-3′′for *Ifnb1*; 5′-GGCTCGCAGGGATGATTTCAA-3′ and 5′-CCAAGTGCTGCCGTCATTTTC-3′ for *Cxcl10*; 5′-AAGAGTCCCCTGCGATTATTTG-3′ and 5′-TCTGGATGGCGTTTGAATTGG-3′ for *Zbp1* and 5′-GGCTGTATTCCCCTCCATCG-3′ and 5′-CCA GTTGGTAACAATGCCATGT-3′ for *Actin*.

Microarray—The microarray was performed in the Hartwell Center of St. Jude Children's Research Hospital from the RNA extracted from untreated naïve BMDMs with TRIzol (Invitrogen, 15596026). The quality of the initial RNA was assessed by running on the Agilent 2100 Bioanalyzer using the nano reagent kit. The concentration was determined by nanodrop, and then 125 ng of intact high-quality RNA was processed using Thermo Fisher (Affymetrix) Whole Transcript (WT) Plus assay kit (Cat# 902280), resulting in fragmented labelled cDNA. This labelled cDNA was included in a hybridization mix that was incubated on the Clariom S mouse array for 16 h at 45°C while rotating at 60 rpm. The cartridges were stained and washed on the Gene Chip FS450 fluidics station and then scanned on the Gene Chip Scanner 3000 7G.

Bioinformatic analysis—BMDM RNAseq data from GSE86922 (unstimulated samples) (Philip et al., 2016) were used. The raw FASTQ file was trimmed by Trim Galore (https://github.com/FelixKrueger/TrimGalore) with quality score 35, mapped to the mouse genome (GRCm38) using STAR 2.7.3a with quantMode TranscriptomeSAM, and the count table was generated by RSEM 1.3.0 rsem-calculate-expression function. Normalization and differentially expressed genes (DEGs) were calculated by the DEseq2 package.

The microarray data were obtained from our in house microarray analysis to compare *Casp8*$^{-/-}$*Ripk3*$^{-/-}$, *Ripk3*$^{-/-}$ and *Casp8*$^{-/-}$*Ripk3*$^{-/-}$*Ripk1*$^{-/-}$ mice and from GEO (GSE137281) to compare *Casp8*$^{\Delta IEC-KO}$ (referred to as *Vil1*-cre × *Casp8*$^{fl/fl}$) mice versus *Casp8*$^{fl/fl}$ mice (Schwarzer et al., 2020). These samples were collected from the colon tissue with 10 samples for *Vil1*-cre × *Casp8*$^{fl/fl}$ due to stronger variation of the colitis phenotype and 5 samples for *Casp8*$^{fl/fl}$ considered as the control group. The raw microarray data were compiled in R (v4.1.1) using the 'oligo' package (Carvalho and Irizarry, 2010) which performed background correction, quantile normalization and $\log_2$ transformation to generate the final dataset for downstream differential expression analysis. The 'limma' package (Ritchie et al., 2015) was used to perform differential expression analysis. Gene set enrichment analysis (GSEA) (Mootha et al., 2003) was performed using the 'fgsea' package (Korotkevich et al., 2021) for the Type-I Interferon signalling pathway (Reactome Id: R-HSA-909733).

For single cell analysis, the data (GSE132133) (Newton et al., 2019b) from whole intestines of E18.5 embryos (one E18.5 *Mlkl*$^{-/-}$ and one *Casp8*$^{C362A/C362A}$*Mlkl*$^{-/-}$, referred to as *Casp8*^{CA}*Mlkl*$^{-/-}$) were available in a gene-barcode matrix format. A total of 1,478 cells

from the *Mlkl*$^{-/-}$ intestine and 1,014 cells from the *Casp8*$^{C362A/C362A}$*Mlkl*$^{-/-}$ intestine were available. Cells were filtered as previously described (Newton et al., 2019b); briefly, for the *Mlkl*$^{-/-}$ sample, cells were included if the number of unique genes detected per cell was between 500 and 3,500, while for the *Casp8*^{CA}*Mlkl*$^{-/-}$ sample, cells were included if the number of unique genes detected per cell was between 300 and 3,000, and the percentage of mitochondrial reads <4%. This resulted in 1,374 *Mlkl*$^{-/-}$ cells and 893 *Casp8*^{CA}*Mlkl*$^{-/-}$ cells. Samples were integrated using the standard integration workflow of 'Seurat' package (v4.0.4) with default parameters to identify cell types common to both samples. Additionally, dimensionality reduction and visualization of the normalized and scaled data were performed using Unified Manifold Approximation and Projection (UMAP). The cell types in the different clusters were assessed using marker genes reported in the adult mouse intestine (Haber et al., 2017). The average expression of different genes in each cell type for the two samples of interest was compared, and cell type specific differential expression analysis (comparing *Casp8*^{CA}*Mlkl*$^{-/-}$ versus *Mlkl*$^{-/-}$) was performed using the 'FindMarkers' function with parameters *min.pct = 0* and *logfc.threshold = 0*. This was done to have a comprehensive list of genes as background when performing downstream GSEA as aforementioned.

QUANTIFICATION AND STATISTICAL ANALYSIS

GraphPad Prism v9.0 software was used for data analysis. Statistical significance was determined by t-test between two groups or one- or two-way ANOVA with Dunnett correction for three or more groups. *p < 0.05, **p < 0.01, ***p < 0.001 and ****p < 0.0001. Data are presented as mean ± SEM. Statistical information for each experiment is found in the figure legends.

Supplementary Material

Refer to Web version on PubMed Central for supplementary material.

ACKNOWLEDGMENTS

We thank all members of the Kanneganti lab for discussions. We also thank R. Tweedell, PhD, and J. Gullett, PhD, for scientific editing and writing support. We thank Drs. Vishva M. Dixit and Nobuhiko Kayagaki (Genentech) for the *Casp11*$^{-/-}$ mouse strain, Dr. Masahiro Yamamoto for the *Ticam1*$^{-/-}$ (*Trif*$^{-/-}$) mutant mouse strain, Dr. Michael Gale for the *Mavs*$^{-/-}$ mutant mouse strain, and Drs. Peter Gough and John Bertin for the *Ripk1* KD mice. We thank the Hartwell Center, a St. Jude Children's Research Hospital facility, which is supported by the National Cancer Institute of the National Institutes of Health under award number P30 CA021765. Research in the Kanneganti lab is supported by grants from the US National Institutes of Health (AI101935, AI124346, AI160179, AR056296, and CA253095) and the American Lebanese Syrian Associated Charities to T.-D.K. The content is solely the responsibility of the authors and does not necessarily represent the official views of the National Institutes of Health.

REFERENCES

Bala Bhaskara Rao K, Katragunta K, Sarma UM, and Jain N (2019). Abundance of d-2-hydroxyglutarate in G2/M is determined by FOXM1 in mutant IDH1-expressing cells. FEBS Lett. 593, 2177–2193. [PubMed: 31211872]

Barrat FJ, Crow MK, and Ivashkiv LB (2019). Interferon target-gene expression and epigenomic signatures in health and disease. Nat. Immunol. 20, 1574–1583. [PubMed: 31745335]

Berger SB, Kasparcova V, Hoffman S, Swift B, Dare L, Schaeffer M, Capriotti C, Cook M, Finger J, Hughes-Earle A, et al. (2014). Cutting Edge: RIP1 kinase activity is dispensable for normal development but is a key regulator of inflammation in SHARPIN-deficient mice. J. Immunol. 192, 5476–5480. [PubMed: 24821972]

Bergeron L, Perez GI, Macdonald G, Shi L, Sun Y, Jurisicova A, Varmuza S, Latham KE, Flaws JA, Salter JC, et al. (1998). Defects in regulation of apoptosis in caspase-2-deficient mice. Genes Dev. 12, 1304–1314. [PubMed: 9573047]

Carvalho BS, and Irizarry RA (2010). A framework for oligonucleotide microarray preprocessing. Bioinformatics 26, 2363–2367. [PubMed: 20688976]

Chen H, Ning X, and Jiang Z (2017). Caspases control antiviral innate immunity. Cell. Mol. Immunol. 14, 736–747. [PubMed: 28690332]

Chen X, Zhu R, Zhong J, Ying Y, Wang W, Cao Y, Cai H, Li X, Shuai J, and Han J (2022). Mosaic composition of RIP1-RIP3 signalling hub and its role in regulating cell death. Nat. Cell Biol. 24, 471–482. [PubMed: 35256774]

Christgen S, Zheng M, Kesavardhana S, Karki R, Malireddi RKS, Banoth B, Place DE, Briard B, Sharma BR, Tuladhar S, et al. (2020). Identification of the PANoptosome: a molecular platform triggering pyroptosis, apoptosis, and necroptosis (PANoptosis). Front. Cell. Infect. Microbiol 10, 237. [PubMed: 32547960]

Chun HJ, Zheng L, Ahmad M, Wang J, Speirs CK, Siegel RM, Dale JK, Puck J, Davis J, Hall CG, et al. (2002). Pleiotropic defects in lymphocyte activation caused by caspase-8 mutations lead to human immunodeficiency. Nature 419, 395–399. [PubMed: 12353035]

Crow MK, Olferiev M, and Kirou KA (2019). Type I interferons in autoimmune disease. Annu. Rev. Pathol. 14, 369–393. [PubMed: 30332560]

Dillon CP, Oberst A, Weinlich R, Janke LJ, Kang TB, Ben-Moshe T, Mak TW, Wallach D, and Green DR (2012). Survival function of the FADD-CASPASE-8-cFLIP(L) complex. Cell Rep. 1, 401–407. [PubMed: 22675671]

Dillon CP, Weinlich R, Rodriguez DA, Cripps JG, Quarato G, Gurung P, Verbist KC, Brewer TL, Llambi F, Gong YN, et al. (2014). RIPK1 blocks early postnatal lethality mediated by caspase-8 and RIPK3. Cell 157, 1189–1202. [PubMed: 24813850]

Dobin A, Davis CA, Schlesinger F, Drenkow J, Zaleski C, Jha S, Batut P, Chaisson M, and Gingeras TR (2013). STAR: ultrafast universal RNA-seq aligner. Bioinformatics 29, 15–21. [PubMed: 23104886]

Durbin JE, Hackenmiller R, Simon MC, and Levy DE (1996). Targeted disruption of the mouse Stat1 gene results in compromised innate immunity to viral disease. Cell 84, 443–450. [PubMed: 8608598]

Fitzgerald KA, McWhirter SM, Faia KL, Rowe DC, Latz E, Golenbock DT, Coyle AJ, Liao SM, and Maniatis T (2003). IKKepsilon and TBK1 are essential components of the IRF3 signaling pathway. Nat. Immunol. 4, 491–496. [PubMed: 12692549]

Gough DJ, Messina NL, Clarke CJP, Johnstone RW, and Levy DE (2012). Constitutive type I interferon modulates homeostatic balance through tonic signaling. Immunity 36, 166–174. [PubMed: 22365663]

Gullett JM, Tweedell RE, and Kanneganti TD (2022). It's all in the PAN: crosstalk, plasticity, redundancies, switches, and interconnectedness encompassed by PANoptosis underlying the totality of cell death-associated biological effects. Cells 11, 1495. [PubMed: 35563804]

Gurung P, Anand PK, Malireddi RKS, Vande Walle L, Van Opdenbosch N, Dillon CP, Weinlich R, Green DR, Lamkanfi M, and Kanneganti TD (2014). FADD and caspase-8 mediate priming and activation of the canonical and noncanonical Nlrp3 inflammasomes. J. Immunol. 192, 1835–1846. [PubMed: 24453255]

Haber AL, Biton M, Rogel N, Herbst RH, Shekhar K, Smillie C, Burgin G, Delorey TM, Howitt MR, Katz Y, et al. (2017). A single-cell survey of the small intestinal epithelium. Nature 551, 333–339. [PubMed: 29144463]

Hakem R, Hakem A, Duncan GS, Henderson JT, Woo M, Soengas MS, Elia A, de la Pompa JL, Kagi D, Khoo W, et al. (1998). Differential requirement for caspase 9 in apoptotic pathways in vivo. Cell 94, 339–352. [PubMed: 9708736]

Hao Y, Hao S, Andersen-Nissen E, Mauck WM 3rd, Zheng S, Butler A, Lee MJ, Wilk AJ, Darby C, Zager M, et al. (2021). Integrated analysis of multimodal single-cell data. Cell 184, 3573–3587.e29. [PubMed: 34062119]

Hughes MA, Harper N, Butterworth M, Cain K, Cohen GM, and Mac-Farlane M (2009). Reconstitution of the death-inducing signaling complex reveals a substrate switch that determines CD95-mediated death or survival. Mol. Cell 35, 265–279. [PubMed: 19683492]

Hwang S, Alhatlani B, Arias A, Caddy SL, Christodoulou C, Bragazzi Cunha J, Emmott E, Gonzalez-Hernandez M, Kolawole A, Lu J, et al. (2014). Murine norovirus: propagation, quantification, and genetic manipulation. Curr. Protoc. Microbiol. 33, 15K.21–61.

Ivashkiv LB, and Donlin LT (2014). Regulation of type I interferon responses. Nat. Rev. Immunol. 14, 36–49. [PubMed: 24362405]

Kaiser WJ, Upton JW, Long AB, Livingston-Rosanoff D, Daley-Bauer LP, Hakem R, Caspary T, and Mocarski ES (2011). RIP3 mediates the embryonic lethality of caspase-8-deficient mice. Nature 471, 368–372. [PubMed: 21368762]

Kamphuis E, Junt T, Waibler Z, Forster R, and Kalinke U (2006). Type I interferons directly regulate lymphocyte recirculation and cause transient blood lymphopenia. Blood 108, 3253–3261. [PubMed: 16868248]

Kang S, Fernandes-Alnemri T, Rogers C, Mayes L, Wang Y, Dillon C, Roback L, Kaiser W, Oberst A, Sagara J, et al. (2015). Caspase-8 scaffolding function and MLKL regulate NLRP3 inflammasome activation downstream of TLR3. Nat. Commun. 6, 7515. [PubMed: 26104484]

Kang TB, Jeong JS, Yang SH, Kovalenko A, and Wallach D (2018). Caspase-8 deficiency in mouse embryos triggers chronic RIPK1-dependent activation of inflammatory genes, independently of RIPK3. Cell Death Differ. 25, 1107–1117. [PubMed: 29666472]

Karki R, Lee S, Mall R, Pandian N, Wang Y, Sharma BR, Malireddi RS, Yang D, Trifkovic S, Steele JA, et al. (2022). ZBP1-dependent inflammatory cell death, PANoptosis, and cytokine storm disrupt IFN therapeutic efficacy during coronavirus infection. Sci. Immunol 7, eabo6294. [PubMed: 35587515]

Karki R, Sharma BR, Tuladhar S, Williams EP, Zalduondo L, Samir P, Zheng M, Sundaram B, Banoth B, Malireddi RKS, et al. (2021a). Synergism of TNF-α and IFN-γ triggers inflammatory cell death, tissue damage, and mortality in SARS-CoV-2 infection and cytokine shock syndromes. Cell 184, 149–168.e17. [PubMed: 33278357]

Karki R, Sundaram B, Sharma BR, Lee S, Malireddi RKS, Nguyen LN, Christgen S, Zheng M, Wang Y, Samir P, et al. (2021b). ADAR1 restricts ZBP1-mediated immune response and PANoptosis to promote tumorigenesis. Cell Rep. 37, 109858. [PubMed: 34686350]

Karst SM, Wobus CE, Lay M, Davidson J, and Virgin HW 4th. (2003). STAT1-dependent innate immunity to a Norwalk-like virus. Science 299, 1575–1578. [PubMed: 12624267]

Kayagaki N, Warming S, Lamkanfi M, Vande Walle L, Louie S, Dong J, Newton K, Qu Y, Liu J, Heldens S, et al. (2011). Non-canonical inflammasome activation targets caspase-11. Nature 479, 117–121. [PubMed: 22002608]

Kelliher MA, Grimm S, Ishida Y, Kuo F, Stanger BZ, and Leder P (1998). The death domain kinase RIP mediates the TNF-induced NF-kappaB signal. Immunity 8, 297–303. [PubMed: 9529147]

Kesavardhana S, Malireddi RKS, and Kanneganti TD (2020). Caspases in cell death, inflammation, and pyroptosis. Annu. Rev. Immunol. 38, 567–595. [PubMed: 32017655]

Korotkevich G, Sukhov V, Budin N, Shpak B, Artyomov MN, and Sergushichev A (2021). Fast gene set enrichment analysis. Preprint at bioRxiv. 10.1101/060012.

Kovalenko A, Kim JC, Kang TB, Rajput A, Bogdanov K, Dittrich-Breiholz O, Kracht M, Brenner O, and Wallach D (2009). Caspase-8 deficiency in epidermal keratinocytes triggers an inflammatory skin disease. J. Exp. Med. 206, 2161–2177. [PubMed: 19720838]

Kumar H, Kawai T, Kato H, Sato S, Takahashi K, Coban C, Yamamoto M, Uematsu S, Ishii KJ, Takeuchi O, et al. (2006). Essential role of IPS-1 in innate immune responses against RNA viruses. J. Exp. Med. 203, 1795–1803. [PubMed: 16785313]

Kuriakose T, Man SM, Malireddi RKS, Karki R, Kesavardhana S, Place DE, Neale G, Vogel P, and Kanneganti TD (2016). ZBP1/DAI is an innate sensor of influenza virus triggering the NLRP3

inflammasome and programmed cell death pathways. Sci. Immunol. 1, aag2045. [PubMed: 27917412]

Lakhani SA, Masud A, Kuida K, Porter GA Jr., Booth CJ, Mehal WZ, Inayat I, and Flavell RA (2006). Caspases 3 and 7: key mediators of mitochondrial events of apoptosis. Science 311, 847–851. [PubMed: 16469926]

Lalaoui N, Boyden SE, Oda H, Wood GM, Stone DL, Chau D, Liu L, Stoffels M, Kratina T, Lawlor KE, et al. (2020). Mutations that prevent caspase cleavage of RIPK1 cause autoinflammatory disease. Nature 577, 103–108. [PubMed: 31827281]

Lee S, Karki R, Wang Y, Nguyen LN, Kalathur RC, and Kanneganti TD (2021). AIM2 forms a complex with pyrin and ZBP1 to drive PANoptosis and host defence. Nature 597, 415–419. [PubMed: 34471287]

Lehtonen A, Matikainen S, and Julkunen I (1997). Interferons up-regulate STAT1, STAT2, and IRF family transcription factor gene expression in human peripheral blood mononuclear cells and macrophages. J. Immunol. 159, 794–803. [PubMed: 9218597]

Li B, and Dewey CN (2011). RSEM: accurate transcript quantification from RNA-Seq data with or without a reference genome. BMC Bioinf. 12, 323.

Lin Y, Devin A, Rodriguez Y, and Liu ZG (1999). Cleavage of the death domain kinase RIP by caspase-8 prompts TNF-induced apoptosis. Genes Dev. 13, 2514–2526. [PubMed: 10521396]

Liu BC, Sarhan J, Panda A, Muendlein HI, Ilyukha V, Coers J, Yamamoto M, Isberg RR, and Poltorak A (2018). Constitutive interferon maintains GBP expression required for release of bacterial components upstream of pyroptosis and anti-DNA responses. Cell Rep. 24, 155–168.e5. [PubMed: 29972777]

Love MI, Huber W, and Anders S (2014). Moderated estimation of fold change and dispersion for RNA-seq data with DESeq2. Genome Biol. 15, 550. [PubMed: 25516281]

Malireddi RKS, Gurung P, Kesavardhana S, Samir P, Burton A, Mummareddy H, Vogel P, Pelletier S, Burgula S, and Kanneganti TD (2020). Innate immune priming in the absence of TAK1 drives RIPK1 kinase activity-independent pyroptosis, apoptosis, necroptosis, and inflammatory disease. J. Exp. Med. 217, e20191644. [PubMed: 31869420]

Malireddi RKS, Gurung P, Mavuluri J, Dasari TK, Klco JM, Chi H, and Kanneganti TD (2018). TAK1 restricts spontaneous NLRP3 activation and cell death to control myeloid proliferation. J. Exp. Med. 215, 1023–1034. [PubMed: 29500178]

Man SM, Karki R, Sasai M, Place DE, Kesavardhana S, Temirov J, Frase S, Zhu Q, Malireddi RKS, Kuriakose T, et al. (2016). IRGB10 liberates bacterial ligands for sensing by the AIM2 and caspase-11-NLRP3 inflammasomes. Cell 167, 382–396.e17. [PubMed: 27693356]

Marié IJ, Brambilla L, Azzouz D, Chen Z, Baracho GV, Arnett A, Li HS, Liu W, Cimmino L, Chattopadhyay P, et al. (2021). Tonic interferon restricts pathogenic IL-17-driven inflammatory disease via balancing the microbiome. Elife 10, e68371. [PubMed: 34378531]

McNab F, Mayer-Barber K, Sher A, Wack A, and O'Garra A (2015). Type I interferons in infectious disease. Nat. Rev. Immunol. 15, 87–103. [PubMed: 25614319]

Mootha VK, Lindgren CM, Eriksson KF, Subramanian A, Sihag S, Lehar J, Puigserver P, Carlsson E, Ridderstråle M, Laurila E, et al. (2003). PGC-1alpha-responsive genes involved in oxidative phosphorylation are coordinately downregulated in human diabetes. Nat. Genet. 34, 267–273. [PubMed: 12808457]

Müller U, Steinhoff U, Reis LF, Hemmi S, Pavlovic J, Zinkernagel RM, and Aguet M (1994). Functional role of type I and type II interferons in antiviral defense. Science 264, 1918–1921. [PubMed: 8009221]

Newton K, Sun X, and Dixit VM (2004). Kinase RIP3 is dispensable for normal NF-kappa Bs, signaling by the B-cell and T-cell receptors, tumor necrosis factor receptor 1, and Toll-like receptors 2 and 4. Mol. Cell Biol. 24, 1464–1469. [PubMed: 14749364]

Newton K, Wickliffe KE, Dugger DL, Maltzman A, Roose-Girma M, Dohse M, Kőműves L, Webster JD, and Dixit VM (2019a). Cleavage of RIPK1 by caspase-8 is crucial for limiting apoptosis and necroptosis. Nature 574, 428–431. [PubMed: 31511692]

Newton K, Wickliffe KE, Maltzman A, Dugger DL, Reja R, Zhang Y, Roose-Girma M, Modrusan Z, Sagolla MS, Webster JD, et al. (2019b). Activity of caspase-8 determines plasticity between cell death pathways. Nature 575, 679–682. [PubMed: 31723262]

Ning X, Wang Y, Jing M, Sha M, Lv M, Gao P, Zhang R, Huang X, Feng JM, and Jiang Z (2019). Apoptotic caspases suppress type I interferon production via the cleavage of cGAS, MAVS, and IRF3. Mol. Cell 74, 19–31.e7. [PubMed: 30878284]

Oberst A, Dillon CP, Weinlich R, McCormick LL, Fitzgerald P, Pop C, Hakem R, Salvesen GS, and Green DR (2011). Catalytic activity of the caspase-8-FLIP(L) complex inhibits RIPK3-dependent necrosis. Nature 471, 363–367. [PubMed: 21368763]

Orning P, and Lien E (2021). Multiple roles of caspase-8 in cell death, inflammation, and innate immunity. J. Leukoc. Biol. 109, 121–141. [PubMed: 32531842]

Orozco S, Yatim N, Werner MR, Tran H, Gunja SY, Tait SWG, Albert ML, Green DR, and Oberst A (2014). RIPK1 both positively and negatively regulates RIPK3 oligomerization and necroptosis. Cell Death Differ. 21, 1511–1521. [PubMed: 24902904]

Philip NH, DeLaney A, Peterson LW, Santos-Marrero M, Grier JT, Sun Y, Wynosky-Dolfi MA, Zwack EE, Hu B, Olsen TM, et al. (2016). Activity of uncleaved caspase-8 controls anti-bacterial immune defense and TLR-induced cytokine production independent of cell death. PLoS Pathog. 12, e1005910. [PubMed: 27737018]

Pomerantz JL, and Baltimore D (1999). NF-kappaB activation by a signaling complex containing TRAF2, TANK and TBK1, a novel IKK-related kinase. EMBO J. 18, 6694–6704. [PubMed: 10581243]

Pop C, Oberst A, Drag M, Van Raam BJ, Riedl SJ, Green DR, and Salvesen GS (2011). FLIP(L) induces caspase 8 activity in the absence of interdomain caspase 8 cleavage and alters substrate specificity. Biochem. J. 433, 447–457. [PubMed: 21235526]

Rajput A, Kovalenko A, Bogdanov K, Yang SH, Kang TB, Kim JC, Du J, and Wallach D (2011). RIG-I RNA helicase activation of IRF3 transcription factor is negatively regulated by caspase-8-mediated cleavage of the RIP1 protein. Immunity 34, 340–351. [PubMed: 21419663]

Rickard JA, O'Donnell JA, Evans JM, Lalaoui N, Poh AR, Rogers T, Vince JE, Lawlor KE, Ninnis RL, Anderton H, et al. (2014). RIPK1 regulates RIPK3-MLKL-driven systemic inflammation and emergency hematopoiesis. Cell 157, 1175–1188. [PubMed: 24813849]

Ritchie ME, Phipson B, Wu D, Hu Y, Law CW, Shi W, and Smyth GK (2015). Limma powers differential expression analyses for RNA-sequencing and microarray studies. Nucleic Acids Res. 43, e47. [PubMed: 25605792]

Rongvaux A, Jackson R, Harman CCD, Li T, West AP, de Zoete MR, Wu Y, Yordy B, Lakhani SA, Kuan CY, et al. (2014). Apoptotic caspases prevent the induction of type I interferons by mitochondrial DNA. Cell 159, 1563–1577. [PubMed: 25525875]

Sarhan J, Liu BC, Muendlein HI, Weindel CG, Smirnova I, Tang AY, Ilyukha V, Sorokin M, Buzdin A, Fitzgerald KA, et al. (2019). Constitutive interferon signaling maintains critical threshold of MLKL expression to license necroptosis. Cell Death Differ. 26, 332–347. [PubMed: 29786074]

Sauer JD, Sotelo-Troha K, von Moltke J, Monroe KM, Rae CS, Brubaker SW, Hyodo M, Hayakawa Y, Woodward JJ, Portnoy DA, et al. (2011). The N-ethyl-N-nitrosourea-induced Goldenticket mouse mutant reveals an essential function of Sting in the in vivo interferon response to Listeria monocytogenes and cyclic dinucleotides. Infect. Immun. 79, 688–694. [PubMed: 21098106]

Schwarzer R, Jiao H, Wachsmuth L, Tresch A, and Pasparakis M (2020). FADD and caspase-8 regulate gut homeostasis and inflammation by controlling MLKL- and GSDMD-mediated death of intestinal epithelial cells. Immunity 52, 978–993.e6. [PubMed: 32362323]

Shiffman ML, Pockros P, McHutchison JG, Schiff ER, Morris M, and Burgess G (2010). Clinical trial: the efficacy and safety of oral PF-03491390, a pancaspase inhibitor - a randomized placebo-controlled study in patients with chronic hepatitis C. Aliment. Pharmacol. Ther. 31, 969–978. [PubMed: 20163376]

Shiow LR, Rosen DB, Brdicková N, Xu Y, An J, Lanier LL, Cyster JG, and Matloubian M (2006). CD69 acts downstream of interferon-alpha/beta to inhibit S1P1 and lymphocyte egress from lymphoid organs. Nature 440, 540–544. [PubMed: 16525420]

Stefan KL, Kim MV, Iwasaki A, and Kasper DL (2020). Commensal microbiota modulation of natural resistance to virus infection. Cell 183, 1312–1324.e10. [PubMed: 33212011]

Subramanian A, Tamayo P, Mootha VK, Mukherjee S, Ebert BL, Gillette MA, Paulovich A, Pomeroy SL, Golub TR, Lander ES, et al. (2005). Gene set enrichment analysis: a knowledge-based approach for interpreting genome-wide expression profiles. Proc. Natl. Acad. Sci. USA 102, 15545–15550. [PubMed: 16199517]

Suthar MS, Ma DY, Thomas S, Lund JM, Zhang N, Daffis S, Rudensky AY, Bevan MJ, Clark EA, Kaja MK, et al. (2010). IPS-1 is essential for the control of West Nile virus infection and immunity. PLoS Pathog. 6, e1000757. [PubMed: 20140199]

Taft J, Markson M, Legarda D, Patel R, Chan M, Malle L, Richardson A, Gruber C, Martín-Fernández M, Mancini GMS, et al. (2021). Human TBK1 deficiency leads to autoinflammation driven by TNF-induced cell death. Cell 184, 4447–4463.e20. [PubMed: 34363755]

Tummers B, and Green DR (2017). Caspase-8: regulating life and death. Immunol. Rev. 277, 76–89. [PubMed: 28462525]

Van Winkle JA, Robinson BA, Peters AM, Li L, Nouboussi RV, Mack M, and Nice TJ (2018). Persistence of systemic murine norovirus is maintained by inflammatory recruitment of susceptible myeloid cells. Cell Host Microbe 24, 665–676.e4. [PubMed: 30392829]

Vande Walle L, Jiménez Fernández D, Demon D, Van Laethem N, Van Hauwermeiren F, Van Gorp H, Van Opdenbosch N, Kayagaki N, and Lamkanfi M (2016). Does caspase-12 suppress inflammasome activation? Nature 534, E1–E4. [PubMed: 27251234]

Wang J, Zheng L, Lobito A, Chan FK, Dale J, Sneller M, Yao X, Puck JM, Straus SE, and Lenardo MJ (1999). Inherited human Caspase 10 mutations underlie defective lymphocyte and dendritic cell apoptosis in autoimmune lymphoproliferative syndrome type II. Cell 98, 47–58. [PubMed: 10412980]

Wang Y, Karki R, Zheng M, Kancharana B, Lee S, Kesavardhana S, Hansen BS, Pruett-Miller SM, and Kanneganti TD (2021). Cutting edge: caspase-8 is a linchpin in caspase-3 and gasdermin D activation to control cell death, cytokine release, and host defense during influenza A virus infection. J. Immunol. 207, 2411–2416. [PubMed: 34663620]

White MJ, McArthur K, Metcalf D, Lane RM, Cambier JC, Herold MJ, van Delft MF, Bedoui S, Lessene G, Ritchie ME, et al. (2014). Apoptotic caspases suppress mtDNA-induced STING-mediated type I IFN production. Cell 159, 1549–1562. [PubMed: 25525874]

Xing Y, Wang X, Jameson SC, and Hogquist KA (2016). Late stages of T cell maturation in the thymus involve NF-kappaB and tonic type I interferon signaling. Nat. Immunol. 17, 565–573. [PubMed: 27043411]

Xu D, Jin T, Zhu H, Chen H, Ofengeim D, Zou C, Mifflin L, Pan L, Amin P, Li W, et al. (2018). TBK1 suppresses RIPK1-driven apoptosis and inflammation during development and in aging. Cell 174, 1477–1491.e19. [PubMed: 30146158]

Xu M, Lee EM, Wen Z, Cheng Y, Huang WK, Qian X, Tcw J, Kouznetsova J, Ogden SC, Hammack C, et al. (2016). Identification of small-molecule inhibitors of Zika virus infection and induced neural cell death via a drug repurposing screen. Nat. Med. 22, 1101–1107. [PubMed: 27571349]

Yamamoto M, Sato S, Hemmi H, Hoshino K, Kaisho T, Sanjo H, Takeuchi O, Sugiyama M, Okabe M, Takeda K, et al. (2003). Role of adaptor TRIF in the MyD88-independent toll-like receptor signaling pathway. Science 301, 640–643. [PubMed: 12855817]

Zhang C, Shang G, Gui X, Zhang X, Bai XC, and Chen ZJ (2019). Structural basis of STING binding with and phosphorylation by TBK1. Nature 567, 394–398. [PubMed: 30842653]

Zheng M, Karki R, Vogel P, and Kanneganti TD (2020). Caspase-6 is a key regulator of innate immunity, inflammasome activation, and host defense. Cell 181, 674–687.e13. [PubMed: 32298652]

Zheng TS, Hunot S, Kuida K, Momoi T, Srinivasan A, Nicholson DW, Lazebnik Y, and Flavell RA (2000). Deficiency in caspase-9 or caspase-3 induces compensatory caspase activation. Nat. Med. 6, 1241–1247. [PubMed: 11062535]

Highlights

- Caspase-8 regulates tonic type I IFN in homeostasis through the RIPK1-TBK1 axis
- Caspase-8 inhibits the interaction between RIPK1 and TBK1 to regulate type I IFN
- When caspase-8 is absent, RIPK1 drives pathogenic IFN production and lymphadenopathy
- RIPK1-mediated IFN leads to natural viral resistance when caspase-8 is absent

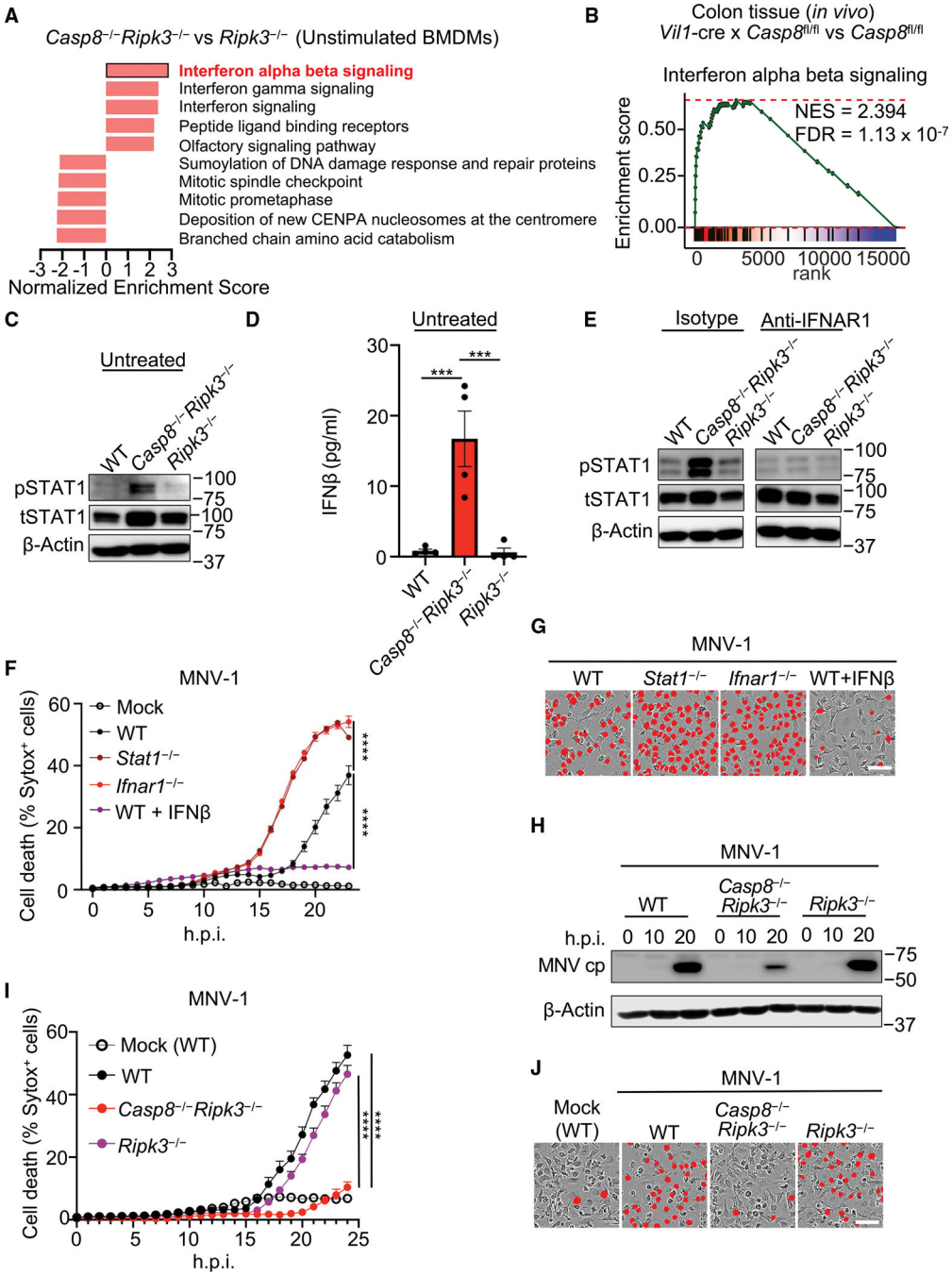

Figure 1. Caspase-8 suppresses spontaneous type I interferon signaling

(A) Gene expression profiling from microarray analysis of untreated *Casp8*$^{-/-}$*Ripk3*$^{-/-}$ and *Ripk3*$^{-/-}$ bone marrow-derived macrophages (BMDMs). The top up- and downregulated REACTOME pathways identified by gene set enrichment analysis (GSEA) are shown.

(B) Enrichment plot of the interferon alpha beta signaling pathway from analysis of publicly available colon tissue RNA-seq data from *Vil1*-cre × *Casp8*$^{fl/fl}$ and *Casp8*$^{fl/fl}$ mice (GEO: GSE137281).

(C) Immunoblots of phosphorylated STAT1 (pSTAT1) and total STAT1 (tSTAT1) from untreated BMDMs from indicated genotypes.
(D) IFNβ concentration in the overnight culture supernatant from untreated BMDMs.
(E) Immunoblots of pSTAT1 and tSTAT1 from untreated or anti-IFNAR1 antibody-treated (10 μg/mL for 12 h) BMDMs.
(F and G) BMDMs were untreated or primed with IFNβ (100 ng/mL) for 1 h, then infected with murine norovirus (MNV-1; multiplicity of infection [MOI] = 10) *in vitro*.
(F) Real-time cell death monitored by Sytox Green staining and quantification.
(G) Representative images of cell death from indicated genotypes at 20 h post-infection (hpi). Scale bar: 50 μm. Red mask denotes dead Sytox Green-positive cells.
(H) Immunoblots of the MNV-1 antigen (MNV cp) in BMDMs of indicated genotypes at indicated hpi (MOI = 10).
(I and J) BMDMs were infected with MNV-1 (MOI = 10) *in vitro*.
(I) Real-time cell death monitored by Sytox Green staining and quantification.
(J) Representative images of cell death from indicated genotypes at 20 hpi. Scale bar: 50 μm. Mean + SEM shown (D, F, and I). (D) ***$p < 0.001$ (one-way ANOVA); (F and I) ****$p < 0.0001$ (two-way ANOVA). β-Actin was used as a loading control. Data are representative of at least three independent experiments (C–J). Molecular weight markers are indicated on the right side of blots. NES, normalized enrichment score; FDR, false discovery rate.

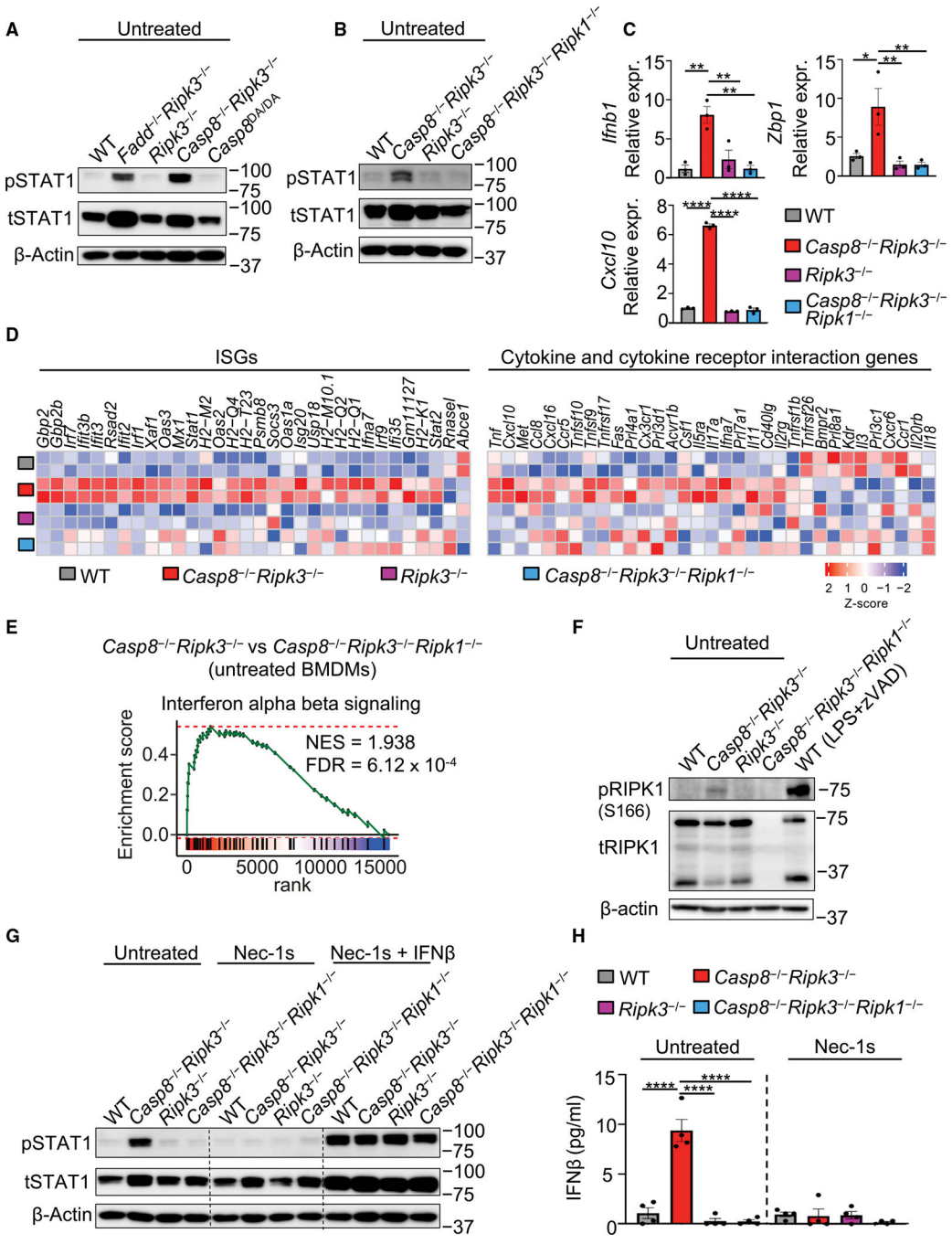

Figure 2. RIPK1 mediates hyperactivation of type I IFN signaling in the absence of caspase-8

(A and B) Immunoblots of pSTAT1 and tSTAT1 in untreated BMDMs from indicated genotypes.

(C) qRT-PCR analysis of *Ifnb1*, *Zbp1*, and *Cxcl10* gene expression from untreated BMDMs of indicated genotypes.

(D and E) Gene expression profiling of microarray results from untreated WT, *Casp8*$^{-/-}$*Ripk3*$^{-/-}$, *Ripk3*$^{-/-}$, and *Casp8*$^{-/-}$*Ripk3*$^{-/-}$*Ripk1*$^{-/-}$ BMDMs. The heatmap of differentially expressed ISGs in the REACTOME interferon alpha beta signaling pathway

(D, left), the heatmap of differentially expressed cytokine and cytokine receptor interaction genes in the KEGG pathway (D, right), and the enrichment plot of the REACTOME interferon alpha beta signaling pathway comparing *Casp8*$^{-/-}$*Ripk3*$^{-/-}$ and *Casp8*$^{-/-}$*Ripk3*$^{-/-}$*Ripk1*$^{-/-}$ BMDMs (E) are shown.

(F) Immunoblots of phosphorylated RIPK1 (pRIPK1 [S166]) and total RIPK1 (tRIPK1) in BMDMs of indicated genotypes. Full-length and cleaved tRIPK1 bands are shown.

(G) Immunoblots of pSTAT1 and tSTAT1 in BMDMs from indicated genotypes left untreated, treated with Nec-1s (50 μM), or treated with Nec-1s (50 μM) and IFNβ (100 ng/mL) for 6 h.

(H) IFNβ concentration in the culture supernatant from BMDMs of indicated genotypes left untreated or treated with Nec-1s (50 μM, overnight).

Mean + SEM shown (C, H). β-Actin was used as a loading control. Data are representative of at least two (F) or three independent experiments. *$p < 0.05$, **$p < 0.01$, ****$p < 0.0001$ (one-way ANOVA). Molecular weight markers are indicated on the right side of blots.

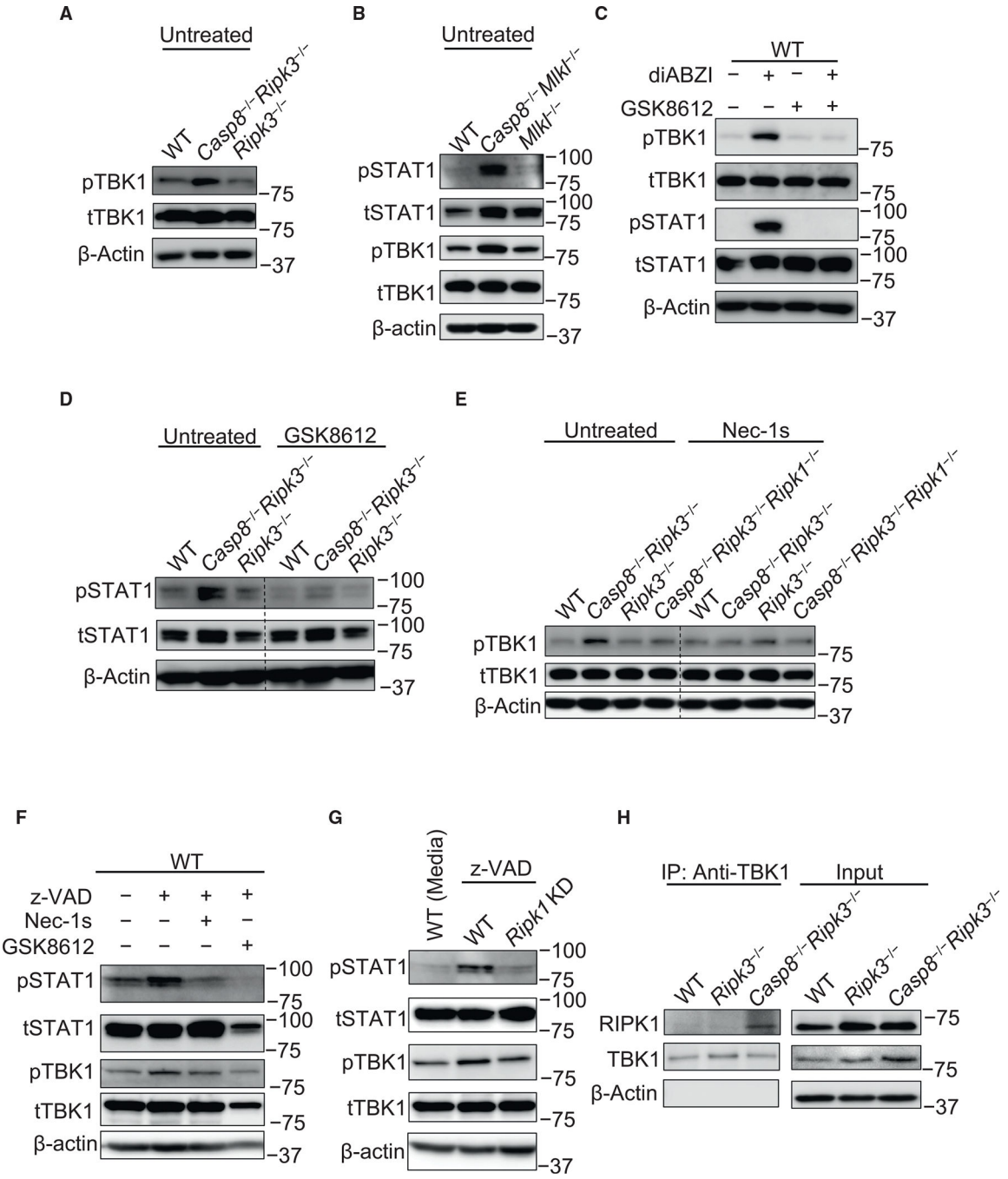

Figure 3. RIPK1 binds to TBK1 and promotes its activation in the absence of caspase-8

(A) Immunoblots of phosphorylated TBK1 (pTBK1) and total TBK1 (tTBK1) in untreated BMDMs of indicated genotypes.

(B) Immunoblots of pSTAT1, tSTAT1, pTBK1, and tTBK1 in untreated BMDMs of indicated genotypes.

(C) Immunoblots of pTBK1, tTBK1, pSTAT1, and tSTAT1 after indicated treatments (diABZI, 5 μM; GSK8612, 25 μM) for 2 h in WT BMDMs.

(D) Immunoblots of pSTAT1 and tSTAT1 in BMDMs of indicated genotypes with or without the TBK1 inhibitor GSK8612 (25 μM) for 12 h.
(E) Immunoblots of pTBK1 and tTBK1 in BMDMs of indicated genotypes with or without the RIPK1 inhibitor Nec-1s (50 μM) for 12 h.
(F and G) Immunoblots of pSTAT1, tSTAT1, pTBK1, and tTBK1 in BMDMs treated with z-VAD (25 μM), Nec-1s (50 μM), or GSK8612 (25 μM) in indicated genotypes for 8 h.
(H) Immunoprecipitation of TBK1 in untreated BMDMs from indicated genotypes. Immunoblots were performed for TBK1, RIPK1, and actin.
β-Actin was used as a loading control. Data are representative of at least three independent experiments. Molecular weight markers are indicated on the right side of blots.

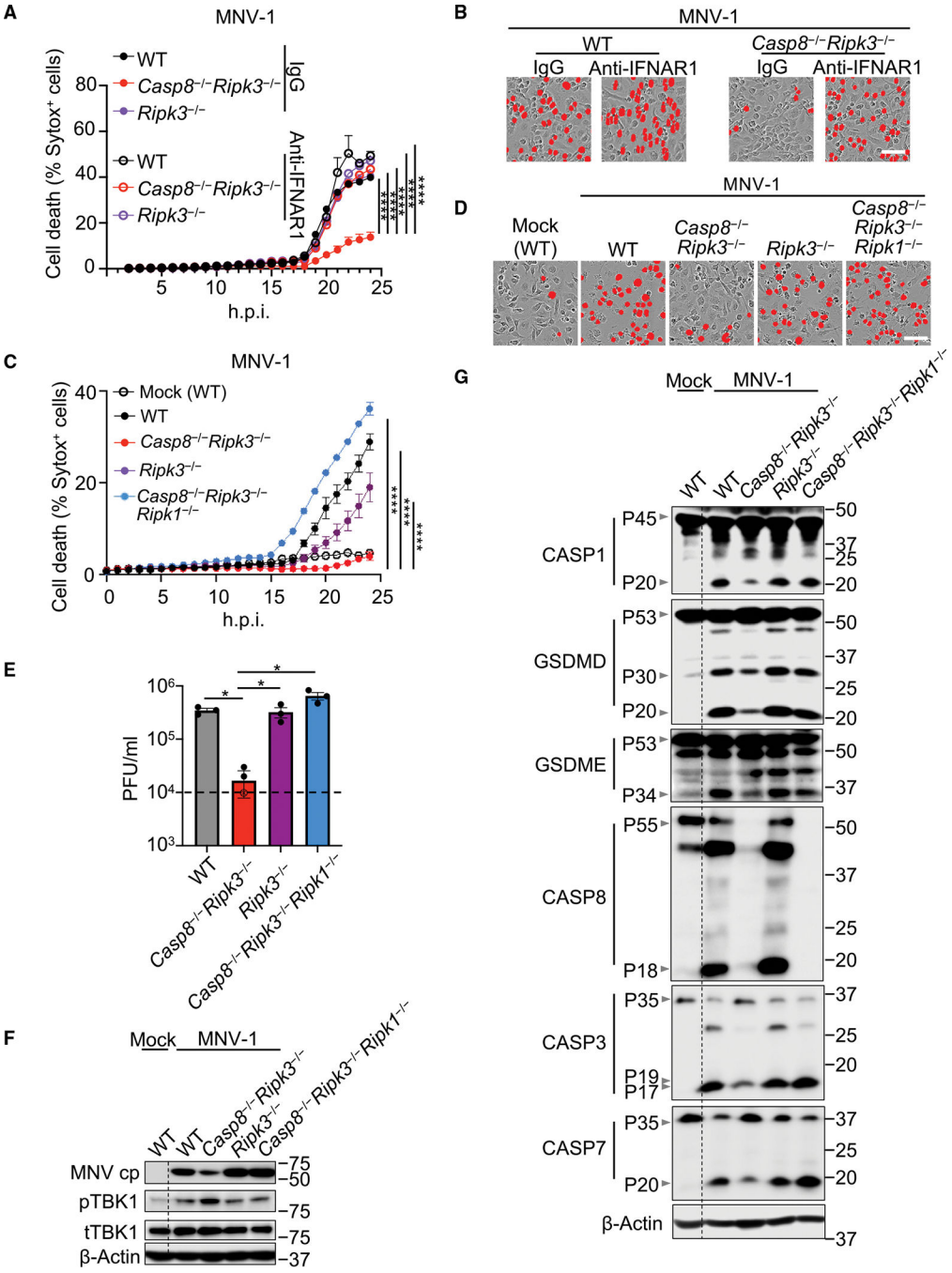

Figure 4. RIPK1-mediated IFN production suppresses virus-induced cell death

(A–D) BMDMs were pre-treated with 10 μg/mL anti-IFNAR1 blocking antibody or IgG for 1 h (A and B) or left untreated (C and D), then infected with MNV-1 (MOI = 10) *in vitro*. Real-time cell death was monitored by Sytox Green staining and quantification (A and C). Mean + SEM shown. ****p < 0.001 (two-way ANOVA).

(B and D) Representative images of cell death from indicated genotypes at 24 hpi. Scale bar: 50 μm. Red mask denotes dead Sytox Green-positive cells.

(E) Plaque assay for MNV-1 viral plaques from the BMDM culture supernatant of indicated genotypes at 24 hpi. Mean + SEM shown. Dotted line is the limit of detection; open circles denote samples with no plaques. *$p < 0.05$ (one-way ANOVA).
(F) Immunoblots of the MNV-1 antigen (MNV cp), pTBK1, and tTBK1 in BMDMs of indicated genotypes at 18 hpi.
(G) Immunoblot analysis of pro- (P45) and activated (P20) caspase-1 (CASP1), pro- (P53), activated (P30), and inactivated (P20) gasdermin D (GSDMD), pro- (P53) and activated (P34) gasdermin E (GSDME), pro- (P55) and cleaved caspase-8 (CASP8; P18), pro- (P35) and cleaved caspase-3 (CASP3; P19 and P17), and pro- (P35) and cleaved caspase-7 (CASP7; P20) of BMDMs of the indicated genotypes at 24 hpi.
β-Actin was used as a loading control. Data are representative of three independent experiments. Molecular weight markers are indicated on the right side of blots.

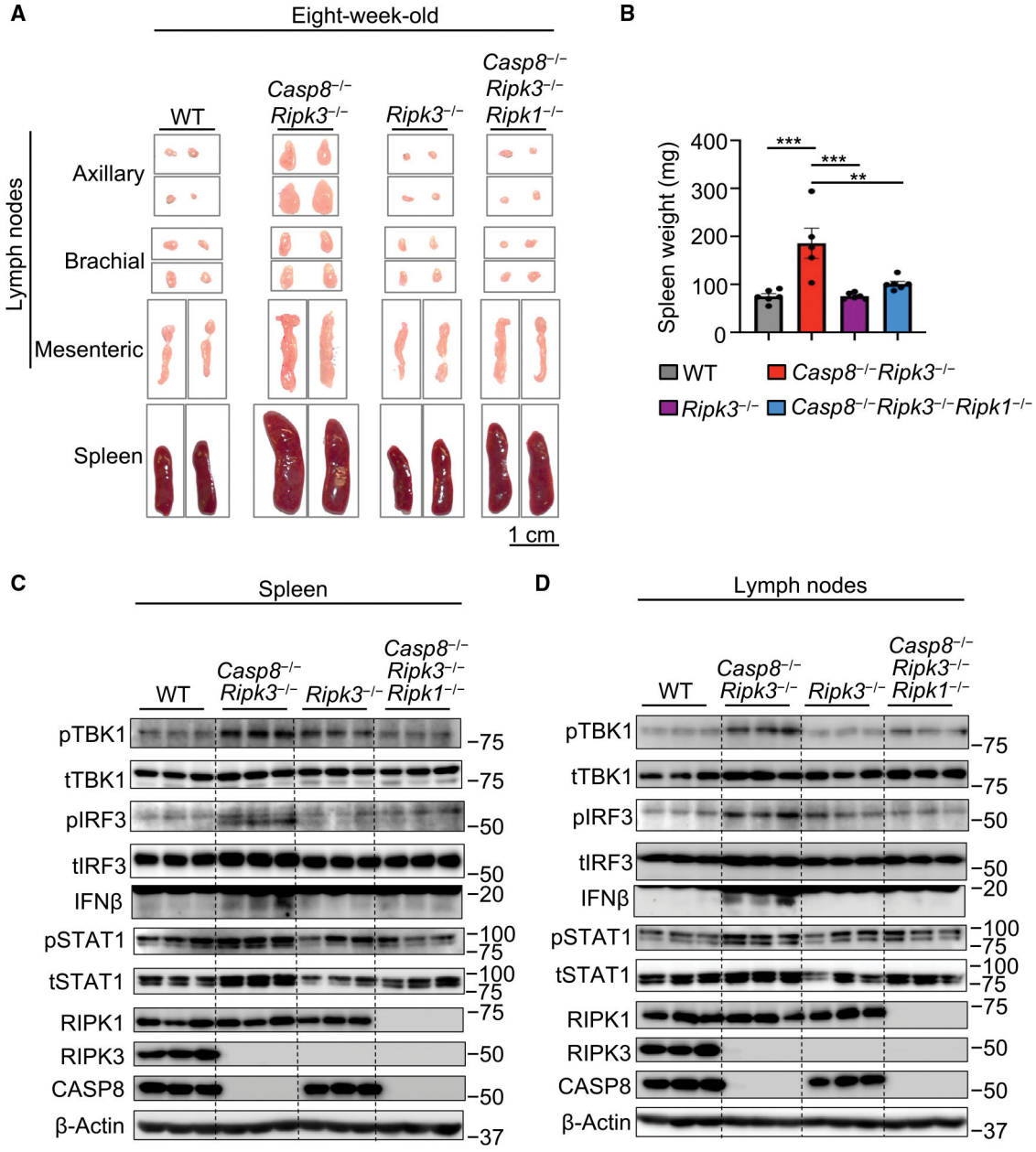

Figure 5. RIPK1 contributes to early lymphadenopathy in caspase-8-deficient mice

(A) Representative images of lymph nodes and spleens from 8-week-old naive WT (n = 6), *Casp8*$^{-/-}$*Ripk3*$^{-/-}$ (n = 5), *Ripk3*$^{-/-}$ (n = 6), and *Casp8*$^{-/-}$*Ripk3*$^{-/-}$*Ripk1*$^{-/-}$ (n = 6) mice.

(B) Spleen weight quantification of 8-week-old naive mice from indicated genotypes.

(C and D) Immunoblots of pTBK1, tTBK1, pIRF3, tIRF3, IFNβ, pSTAT1, tSTAT1, RIPK1, RIPK3, and CASP8 in splenic tissue (C) or lymph node (D) lysates from 8-week-old naive mice of indicated genotypes. Each lane is one animal.

Data are pooled from WT (n = 6), *Casp8*$^{-/-}$*Ripk3*$^{-/-}$ (n = 5), *Ripk3*$^{-/-}$ (n = 6), and *Casp8*$^{-/-}$*Ripk3*$^{-/-}$*Ripk1*$^{-/-}$ (n = 6) mice and presented as mean + SEM (B). **p < 0.01, ***p < 0.001 (one-way ANOVA). Data are representative of two experiments (C and D).

KEY RESOURCES TABLE

REAGENT or RESOURCE	SOURCE	IDENTIFIER
Antibodies		
anti-IFNβ	Leinco	Cat# 1-439; RRID: AB_2737543
anti-caspase-3	Cell Signaling Technology	Cat# 9662; RRID: AB_331439
anti-cleaved caspase-3	Cell Signaling Technology	Cat# 9661; RRID: AB_2341188
anti-caspase-7	Cell Signaling Technology	Cat# 9492; RRID: AB_2228313
anti-cleaved caspase-7	Cell Signaling Technology	Cat# 9491; RRID: AB_2068144
anti-caspase-8	Adipogen	Cat# AG-20T-0138-C100; RRID: AB_2490519
anti-cleaved caspase-8	Cell Signaling Technology	Cat# 8592; RRID: AB_10891784
anti-GSDMD	Abcam	Cat# ab209845; RRID: AB_2783550
anti-GSDME	Abcam	Cat# ab215191; RRID: AB_2737000
anti-caspase-1	AdipoGen	Cat# AG-20B-0044; RRID: AB_2490253
anti-β-Actin	Proteintech	Cat# 66009-1-IG; RRID: AB_2687938
HRP-conjugated secondary anti-rabbit	Jackson ImmunoResearch Laboratories	Cat# 111-035-047; RRID: AB_2337940
HRP-conjugated secondary anti-mouse	Jackson ImmunoResearch Laboratories	Cat# 315-035-047; RRID: AB_2340068
anti-MNV-1 cp	Millipore	Cat# MABF2097-100UG
anti-pTBK1	Cell Signaling Technology	Cat# 5483; RRID: AB_10693472
anti-tTBK1	Cell Signaling Technology	Cat# 3504; RRID: AB_2255663
anti-pSTAT1	Cell Signaling Technology	Cat# 7649; RRID: AB_10950970
anti-tSTAT1	Cell Signaling Technology	Cat# 14994; RRID: AB_2737027
anti-pRIPK1 (S166)	Cell Signaling Technology	Cat# 65746, RRID:AB_2799693
anti-tRIPK1	Cell Signaling Technology	Cat# 3493, RRID:AB_2305314
anti-RIPK3	ProSci	Cat# 2283, RRID:AB_203256
anti-pIRF3	Cell Signaling Technology	Cat# 29047, RRID:AB_2773013
anti-tIRF3	Cell Signaling Technology	Cat# 4302, RRID:AB_1904036
anti-FLAG	Rockland	Cat# 600-401-383, RRID:AB_219374
anti-FLAG	Sigma	Cat# F3165, RRID:AB_259529
anti-HA	Thermo Fisher Scientific	Cat# PA1-985, RRID:AB_559366
anti-IgG1	Cell Signaling Technology	Cat# 5415; RRID: AB_10829607
anti-HA	Millipore	Cat# 05-904; RRID: AB_417380
anti-IFNAR1	Invitrogen	Cat# 16-5945-85; RRID: AB_1210688
Chemicals, peptides, and recombinant proteins		
IMDM	Thermo Fisher Scientific	Cat# 12440053
Fetal bovine serum	Biowest	Cat# S1620
Non-essential amino acids	Thermo Fisher Scientific	Cat# 11140-050
Penicillin and streptomycin	Thermo Fisher Scientific	Cat# 15070-063
DPBS	Thermo Fisher Scientific	Cat# 14190-250
GSK8612	Selleckchem	Cat# S8872

REAGENT or RESOURCE	SOURCE	IDENTIFIER
H151	Selleckchem	Cat# S6652
Nec-1s	Selleckchem	Cat# S8641
diABZI	Selleckchem	Cat# S8796
poly(I:C)	InvivoGen	Cat# tlrl-picw
poly(I:C)	InvivoGen	Cat# tlrl-pic
c-di-GMP	InvivoGen	Cat# tlrl-nacdg
LPS	Sigma	Cat# L2630
z-VAD-FMK	Cayman	Cat# 14463
IFNβ	PBL Assay	Cat# 12400-1
Sytox Green	Thermo Fisher Scientific	Cat# S7020
Protease inhibitor	R&D	Cat# 201-LB-025)
Phosphatase inhibitor	Peprotech	Cat# 315-01A
Protein A/G agarose beads	SantaCruz	Cat# sc-2003
DpnI	NEB	Cat# R0176S
Forte western HRP substrate	Millipore	Cat# WBLUF0500
TRIzol	Invitrogen	Cat# 15596026
DMEM	Thermo Fisher Scientific	Cat# 15596026
OptiMEM	Gibco	Cat# #31985070
Critical commercial assays		
High-Capacity cDNA Reverse Transcription Kit	Thermo Fisher Scientific	Cat# 4368814
Whole Transcript Plus assay kit	Thermo Fisher Scientific	Cat# 902280
Xfect	Takara	Cat# 631318
NEBuilder® HiFi DNA Assembly Cloning Kit	NEB	Cat# E5520S
LEGEND MAX™ Mouse IFN-β ELISA Kit	BioLegend	Cat# #439407
Power SYBR Green PCR Master Mix	Applied Biosystems	Cat# 4367659
Recombinant DNA		
pcDNA-HA	Addgene	Cat#128034
pcDNA-Flag-RIPK1	Addgene	Cat# 78842
Oligonucleotides		
Primers *Ifnbl* sequence (Fwd-CAGCTCCAAGAAAGGACGAAC, Rev-GGCAGTGTAACTCTTCTGCAT)	IDT	N A
Primers *Cxcl10* sequence (Fwd-GGCTCGCAGGGATGATTTCAA, Rev-CCAAGTGCTGCCGTCATTTTC)	IDT	N/A
Primers *Zbp1* sequence (Fwd-AAGAGTCCCCTGCGATTATTTG, Rev-TCTGGATGGCGTTTGAATTGG)	IDT	N/A
Primers *B-actin* sequence (Fwd-GGCTGTATTCCCCTCCATCG, Rev-CCAGTTGGTAACAATGCCATGT)	IDT	N/A
Experimental models: Cell lines		

REAGENT or RESOURCE	SOURCE	IDENTIFIER
RAW264.7	ATCC	Cat# TIB-71
HEK293T	ATCC	Cat# CRL-3216
Experimental models: Organisms/strains		
MNV-1	ATCC	Cat# VR-1937
Casp8$^{-/-}$*Ripk3*$^{-/-}$	(Oberst et al., 2011)	N/A
Fadd$^{-/-}$*Ripk3*$^{-/-}$	(Dillon et al., 2012)	N/A
Ripk3$^{-/-}$	(Newton et al., 2004)	N/A
Casp8$^{D387A/D387A}$	(Wang et al., 2021)	N/A
Ripk1$^{K45A/K45A}$ (*Ripk1* KD)	(Berger et al., 2014)	N/A
Ticam 1 $^{-/-}$	(Yamamoto et al., 2003)	N/A
Mavs$^{-/-}$	(Kumar et al., 2006; Suthar et al., 2010)	N/A
Sting$^{gt/gt}$	(Sauer et al., 2011)	N/A
Stat1$^{-/-}$	(Durbin et al., 1996)	N/A
Ifnar1$^{-/-}$	(Muller et al., 1994)	N/A
Casp1$^{-/-}$	(Man et al., 2016)	N/A
Casp2$^{-/-}$	Jackson Laboratory, 007899 (Bergeron et al., 1998)	N/A
Casp3$^{-/-}$	(Zheng et al., 2000)	N/A
Casp6$^{-/-}$	Jackson Laboratory, 006236 (Zheng et al., 2020)	N/A
Casp7$^{-/-}$	(Lakhani et al., 2006)	N/A
Casp9$^{-/-}$	(Hakem et al., 1998)	N/A
Casp11$^{-/-}$	(Kayagaki et al., 2011)	N/A
Casp12$^{-/-}$	(Vande Walle et al., 2016)	N/A
Ripk1$^{-/-}$	(Kelliher et al., 1998)	N/A
Casp8$^{-/-}$*Ripk3*$^{-/-}$*Ripk1*$^{-/-}$	This study	N/A
Software and algorithms		
GraphPad Prism 8.0	GraphPad Software, Inc.	https://www.graphpad.com/
ImageJ	National Institutes of Health (NIH), USA	https://imagej.nih.gov/ij/download.html
Gene Set Enrichment Analysis (GSEA)	The Broad Institute	https://www.gsea-msigdb.org/gsea/index.jsp
Trim Galore	Babraham Bioinformatics	https://www.bioinformatics.babraham.ac.uk/projects/trim_galore/
STAR 2.7.3a	(Dobin et al., 2013)	https://github.com/alexdobin/STAR/releases
RSEM 1.3.0	(Li and Dewey, 2011)	https://deweylab.github.io/RSEM/
DEseq2	(Love et al., 2014)	https://bioconductor.org/packages/release/bioc/html/DESeq2.html
'oligo' package	(Carvalho and Irizarry, 2010)	https://www.bioconductor.org/packages/release/bioc/html/oligo.html

REAGENT or RESOURCE	SOURCE	IDENTIFIER
'limma' package	(Ritchie et al., 2015)	https://www.bioconductor.org/packages/release/bioc/html/limma.html
'fgsea' package	(Korotkevich et al., 2021)	https://bioconductor.org/packages/release/bioc/html/fgsea.html
'Seurat' package (v4.0.4)	(Hao et al., 2021)	https://cloud.r-project.org/package=Seurat
Deposited data		
BMDM microarray data	This study	GSE211623
Intestine microarray data	(Schwarzer et al., 2020)	GSE137281
BMDM RNAseq data	(Philip et al., 2016)	GSE86922
Single cell RNAseq data	(Newton et al., 2019b)	GSE132133